

**EXPERIMENTAL ANALYSIS OF INKJET
PRINTED MULTI METAL OXIDE
PHOTOELECTRODES FOR WATER SPLITTING
APPLICATIONS**

**A Thesis Submitted to
the Graduate School of
İzmir Institute of Technology
in Partial Fulfillment of the Requirements for the Degree of
MASTER OF SCIENCE
in Materials Science and Engineering**

**by
Gülsüm Efsun TEKNECİ**

**July 2020
İZMİR**

ACKNOWLEDGEMENTS

In the emergence of this scientific study, I would like to point out that the support of the people with expertise in different disciplines that I will mention below is indispensable.

First of all, I would like to thank to my advisor Assoc. Prof. Dr. Engin KARABUDAK, who provided me with the mentality of academic work and supported patiently.

I would also like to thank to my co-advisor Asst. Prof. Dr. Umut ADEM and Assoc. Prof. Dr. Sinan BALCI, Dr. İbrahim İNANÇ for their invaluable contributions.

I am thankful for the support from the members of Karabudak Research Group: Emre Yusuf GÖL, Ahmet AYTEKİN, Özge Sevin KESKİN, Gün Deniz AKKOÇ, Ecem ÖZKAHRAMAN, Ali İhsan KANLI, Mert KOÇ, Mehmet KIVANÇ, Turgut UĞUR and Onur TEKİN.

I would like to thank to Tuğçe Aybüke ARICA GÜVENÇ, Çetin Meriç GÜVENÇ, Ezgi İNCİ and Şengül KAYA for sincerely supporting me in the emergence of this thesis and the challenging interviews I was accepted.

I appreciate Polat BULANIK's and Hüseyin BİLİR's helpfulness in solving the technical problems I experienced.

I am grateful to my best friends Süreyya Aysun ARICAN who owes a large part in the evolution of my journey and Kaniye GÜNEŞ for standing up for me through all the difficulties I faced.

I would like to express my gratitude to my sister Nazar MERMER and Serhat MERMER, who supported me with their unconditional love and understanding from the very beginning.

Lastly, I would deeply thank to my mother Seher TEKNECİ and my father Zeki TEKNECİ for believing in my efforts.

ABSTRACT

EXPERIMENTAL ANALYSIS OF INKJET PRINTED MULTI METAL OXIDE PHOTOELECTRODES FOR WATER SPLITTING APPLICATIONS

Recently, scientific research studies focus on renewable energy solutions as well as energy efficiency in managing the upcoming climate crisis which manifests itself in the form of global warming. However, the chaotic nature of renewable energy sources caused energy storage technologies to gain importance. In addition to battery technologies consisting of lithium and post-lithium ion, zinc-air, nickel-zinc and lead-acid; artificial photosynthesis products such as hydrogen and methanol also show superiority in transportation. Especially hydrogen fuel is in the leading position with gravimetric energy density of approximately 140 MJ/kg. In this study, the experimental procedure is conducted and analyzed to produce cost-effective multi-metal oxide catalysts at high speed and efficiency with a combinatorial approach using inkjet printing technology to obtain hydrogen by splitting water. Considering the abundancies in nature, especially nickel, cobalt, iron, manganese, copper and chromium salts were preferred to obtain oxide derivatives. Inkjet printing experiments were conducted with the printer provided by Sağlık İzleme Sistemleri A.Ş.. The precision of the printed layers was examined and compared with the literature values. In cases involving differences from the literature value, possible causes are emphasized and solutions are suggested. Problems in transition from single metal oxide printed layers to more complicated multi-metal oxide prints have been examined and solutions have been proposed. As a result, this experimental study is aimed to provide foresight for large-scale (photo)electrocatalyst production with the utilization of inkjet printing.

ÖZET

SU AYRIŞTIRMA UYGULAMALARI İÇİN MÜREKKEP PÜSKÜRTME BASKILI ÇOKLU METAL OKSİT FOTOELEKTROTLARIN DENEYSEL ANALİZİ

Günümüzde küresel ısınma şeklinde kendini gösteren, yaklaşmakta olan iklim krizinin yönetilmesinde enerji verimliliğinin yanısıra yenilenebilir enerji çözümlerine odaklanılmaktadır. Bununla birlikte yenilenebilir enerji kaynaklarının kaotik yapısı enerji depolamanın daha fazla önem kazanmasına yol açmıştır. Lityum ve post-lityum iyon, çinko-hava, nikel-çinko ve kurşun-asitten oluşan pil teknolojilerine ek olarak gravimetrik enerji yoğunluğu bu teknolojilerden çok daha fazla olan, hidrojen ve metanol gibi yapay fotosentez ürünleri buna ek olarak taşınabilirlik konusunda da üstünlük göstermektedir. Özellikle hidrojen yakıtı yaklaşık olarak 140 MJ/kg'lık gravimetrik enerji yoğunluğuyla lider konumdadır. Bu çalışmada suyun ayrıştırılmasıyla hidrojen eldesi için mürekkep püskürtme baskı teknolojisi kullanılarak kombinasyonel yaklaşımla düşük maliyetli çoklu metal oksit katalizörlerinin yüksek hız ve verimde üretilmesi için deneysel prosedür incelenmiş ve analiz edilmiştir. Doğada bulunma sıklığı göz önüne alınarak oksit türevlerinin eldesi için özellikle nikel, kobalt, demir, mangan, bakır ve krom tuzları tercih edilmiştir. Mürekkep püskürtme baskı denemelerinin tümü Sağlık İzleme Sistemleri A.Ş. tarafından sağlanan yazıcıyla yapılmıştır. Baskıların hassasiyetleri incelenmiş olup literatür değerleriyle karşılaştırma yapılmıştır. Literatür değerinden farklılıklar içeren durumlarda olası nedenler üzerinde durulmuş ve çözüm yolları önerilmiştir. Tekli metal oksit baskılardan daha komplike olan çoklu metal oksit baskılara geçişte yaşanan problemler incelenmiş ve çözüm önerileri getirilmiştir. Sonuç olarak yapılan deneysel çalışmanın mürekkep püskürtme baskı kullanılarak büyük ölçekli (foto)elektrokatalizör üretimine yönelik öngörü sağlaması hedeflenmiştir.

TABLE OF CONTENTS

LIST OF FIGURES.....	vii
LIST OF TABLES.....	xii
CHAPTER 1. INTRODUCTION.....	1
1.1. Global Energy Supply Problem.....	1
1.2. Global Energy Storage Problem.....	1
1.3. Artificial Photosynthesis.....	2
1.4. Water Splitting.....	2
1.5. State of the Art Catalysts for OER and HER.....	4
1.6. Combinatorial Approach and Inkjet Printing of Catalysts.....	7
1.7. Main Scientific Question.....	7
CHAPTER 2. INKS AS CATALYST PRECURSORS FOR INKJET PRINTING.....	8
2.1. Materials.....	8
2.2. Characterization of the Inks.....	8
2.2.1. Surface Tension.....	8
2.2.1.1. Experimental Procedure.....	8
2.2.1.2. Results and Discussion.....	9
2.2.2. Viscosity.....	10
2.2.2.1. Experimental Procedure.....	10
2.2.2.2. Results and Discussion.....	10
2.2.3. Volatility.....	11
2.2.3.1. Experimental Procedure.....	11
2.2.3.2. Results and Discussion.....	12
CHAPTER 3. EXPERIMENTAL VALIDATION.....	20
3.1. Printer Test Protocol.....	20
3.1.1. Effect of Tray Position.....	20

3.1.1.1. Experimental Procedure.....	20
3.1.1.2. Results and Discussion.....	21
3.1.2. Precision & Accuracy Test.....	22
3.1.2.1. Electrocatalyst Measurement Protocol.....	22
3.1.2.1.1. Experimental Procedure.....	23
3.1.2.1.2. Results and Discussion.....	24
3.1.2.2. Single Metal Oxides.....	27
3.1.2.2.1. Experimental Procedure.....	27
3.1.2.2.2. Results and Discussion.....	28
3.1.2.3. Multi Metal Oxides.....	33
3.1.2.3.1. Compositional Scan of Nickel, Iron and Cobalt Oxides.....	33
3.1.2.3.1.1. Experimental Procedure.....	33
3.1.2.3.1.2. Results and Discussion.....	35
3.1.2.3.2. Compositional Scan of Nickel, Cobalt and Copper Oxides..	37
3.1.2.3.2.1. Experimental Procedure.....	37
3.1.2.3.2.2. Results and Discussion.....	38
3.2. Effect of Film Homogeneity.....	40
3.2.1. Experimental Procedure.....	40
3.2.2. Results and Discussion.....	45
3.3. Comparison with Drop Casting Deposition Technique.....	50
3.3.1. Experimental Procedure.....	50
3.3.2. Results and Discussion.....	51
 CHAPTER 4. CONCLUSIONS AND OUTLOOKS.....	 56
 REFERENCES.....	 58

LIST OF FIGURES

<u>Figure</u>	<u>Page</u>
Figure 2.1. The experimental setup for surface tension measurement of precursor ink.....	9
Figure 2.2. The experimental setup for viscosity measurement of precursor inks.....	10
Figure 2.3. The experimental setup for volatility of precursor inks.....	11
Figure 2.4. The change of percentage due to evaporation for Epson T673 ink with respect to time (0.7 mL out of 14 mL) (inset: evaporation rate).....	12
Figure 2.5. The change of percentage due to evaporation for ethanol with respect to time (5.4 mL out of 14 mL) (inset: evaporation rate).....	12
Figure 2.6. The change of percentage due to evaporation for acetic acid with respect to time (1.8 mL out of 14 mL) (inset: evaporation rate).....	13
Figure 2.7. The change of percentage due to evaporation for SIZ+ inkjet buffer ink for metal salts with respect to time (4 mL out of 14 mL) (inset: evaporation rate).....	13
Figure 2.8. The change of percentage due to evaporation for Ni ink with respect to time (5.5 mL out of 14 mL) (inset: evaporation rate).....	14
Figure 2.9. The change of percentage due to evaporation for Mn ink with respect to time (5.2 mL out of 14 mL) (inset: evaporation rate).....	14
Figure 2.10. The change of percentage due to evaporation for Cu ink with respect to time (6.2 mL out of 14 mL) (inset: evaporation rate).....	15
Figure 2.11. The change of percentage due to evaporation for Cr ink with respect to time (6.3 mL out of 14 mL) (inset: evaporation rate).....	15
Figure 2.12. The change of percentage due to evaporation for Fe ink with respect to time (6.5 mL out of 14 mL) (inset: evaporation rate).....	16
Figure 2.13. The change of percentage due to evaporation for Co ink with respect to time (5.2 mL out of 14 mL) (inset: evaporation rate).....	16
Figure 2.14. The comparison of the change of percentage due to evaporation for all samples with respect to time.....	17
Figure 2.15. Dimensions of the ink containers used.....	17
Figure 2.16. pH measurements of tested samples.....	19
Figure 3.1. Measurement of distance between the inkjet printhead and the tray.....	20

<u>Figure</u>	<u>Page</u>
Figure 3.2. Printed circular patterns with increasing distances.....	21
Figure 3.3. Printed circular patterns with increasing distances after oxidation at 230 °C for 60 minutes.....	21
Figure 3.4. Optical microscopy images for examination of the boundaries.....	22
Figure 3.5. a) Cyclic voltammograms for Pt wire in 1 M KOH electrolyte with a scan rate of 1 mV/s, b) Tafel plots derived from cyclic voltammograms for Pt wire in 1 M KOH electrolyte with a scan rate of 1 mV/s, c) Tafel plot derived from chronopotentiometry for Pt wire in 1 M KOH electrolyte.....	24
Figure 3.6. a) Cyclic voltammograms for Ni foam in 1 M KOH electrolyte with a scan rate of 1 mV/s, b) Tafel plots derived from cyclic voltammograms for Ni foam in 1 M KOH electrolyte with a scan rate of 1 mV/s, c) Tafel plot derived from chronopotentiometry for Ni foam in 1 M KOH electrolyte.....	25
Figure 3.7. a) Cyclic voltammograms for IrO ₂ in 1 M KOH electrolyte with a scan rate of 5 mV/s, b) Tafel plots derived from cyclic voltammograms for IrO ₂ in 1 M KOH electrolyte with a scan rate of 5 mV/s, c) Tafel plot derived from chronopotentiometry for IrO ₂ in 1 M KOH electrolyte.....	26
Figure 3.8. a) Precision of cyclic voltammograms for printed NiO catalysts b) Sequentially printed NiO catalysts c), d) Optical microscopic image with different magnifications printed NiO catalyst.....	28
Figure 3.9. a) Precision of cyclic voltammograms for printed Mn ₃ O ₄ catalysts b) Sequentially printed Mn ₃ O ₄ catalysts c), d) Optical microscopic image with different magnifications printed Mn ₃ O ₄ catalyst.....	29
Figure 3.10. a) Precision of cyclic voltammograms for printed Cr ₂ O ₃ catalysts b) Sequentially printed Cr ₂ O ₃ catalysts c), d) Optical microscopic image with different magnifications printed Cr ₂ O ₃ catalyst.....	29
Figure 3.11. a) Precision of cyclic voltammograms for printed Co ₃ O ₄ catalysts b) Sequentially printed Co ₃ O ₄ catalysts.....	30
Figure 3.12. a) Precision of cyclic voltammograms for printed CuO catalysts b) Sequentially printed CuO catalysts.....	30

<u>Figure</u>	<u>Page</u>
Figure 3.13. a) Precision of cyclic voltammograms for printed Fe ₂ O ₃ catalysts b) Sequentially printed Fe ₂ O ₃ catalysts.....	30
Figure 3.14. (Ni-Fe-Co)O _x compositional scan (@750 mV vs Ag/AgCl) (Reprinted with permission from ACS Comb. Sci. 2014, 16, 2, 47–52. Copyright © 2014, American Chemical Society).....	34
Figure 3.15. Cyclic voltammograms of printed a) Ni _{0.85} Fe _{0.1} Co _{0.05} O _x , b) Ni _{0.45} Fe _{0.15} Co _{0.4} O _x , c) Ni _{0.15} Fe _{0.35} Co _{0.5} O _x catalysts in 0.1 M NaOH electrolyte with a scan rate of 50mV/s.....	35
Figure 3.16. Tray positions for printed NiCoCuO _x catalysts #6 - #10.....	37
Figure 3.17. Cyclic voltammograms of printed Ni _x Co _y Cu _z O _n catalysts in 0.1 M KOH electrolyte with a scan rate of 100mV/s.....	38
Figure 3.18. Forces governing evaporation induced film formation from a droplet. (Reprinted from Advanced Functional Materials, Volume 18, Issue 2, J. A. Lim, W. H. Lee, H. S. Lee, J. H. Lee, Y. D. Park, K. Cho, Self-Organization of Ink-jet-Printed Triisopropylsilylethynyl Pentacene via Evaporation-Induced Flows in a Drying Droplet, Pages 229-234, Copyright © 2008 WILEY-VCH Verlag GmbH & Co. KGaA, Weinheim).....	41
Figure 3.19. Optical microscope (OM) and polarized images of ink-jet-printed TIPS_PEN droplets with various solvent compositions: a) chlorobenzene and mixed-solvents containing chlorobenzene and 25 vol % b) hexane, c) o-dichlorobenzene, and d) dodecane. The height profiles of the TIPS_PEN single dots printed from e) chlorobenzene and the solvent mixture containing chlorobenzene and 25 vol %, f) hexane, and g) dichlorobenzene are shown at the bottom (scale bar = 50 μm). (Reprinted from Advanced Functional Materials, Volume 18, Issue 2, J. A. Lim, W. H. Lee, H. S. Lee, J. H. Lee, Y. D. Park, K. Cho, Self-Organization of Ink-jet-Printed Triisopropylsilylethynyl Pentacene via Evaporation-Induced Flows in a Drying Droplet, Pages 229-234, Copyright © 2008 WILEY-VCH Verlag GmbH & Co. KGaA, Weinheim).....	42

<u>Figure</u>	<u>Page</u>
Figure 3.20. SEM images and surface profiles of Al ₂ O ₃ ink droplets: (a) water single-solvent ink and (b) DMF + water co-solvent ink. (Reprinted from Current Applied Physics, Volume 11, Issue 3, Supplement, Yeonjun Oh, Jihoon Kim, Young Joon Yoon, Hyotae Kim, Ho Gyu Yoon, Sung-Nam Lee, Jonghee Kim, Inkjet printing of Al ₂ O ₃ dots, lines, and films: From uniform dots to uniform films, Pages S359-S363, Copyright © 2011, with permission from Elsevier).....	43
Figure 3.21. a) Sequentially printed NiO catalysts including 0, 10, 25, 50% dodecane, respectively. b), c) Optical microscopic image with different magnifications printed NiO catalyst including 10% dodecane.....	45
Figure 3.22. Contact angle measurement apparatus.....	45
Figure 3.23. Contact angle measurement of pure water before and after silanization of F:SnO ₂ /glass, respectively.....	46
Figure 3.24. Contact angle measurement of Ni ink before and after silanization of F:SnO ₂ /glass, respectively.....	46
Figure 3.25. Contact angle measurement of Mn ink before and after silanization of F:SnO ₂ /glass, respectively.....	47
Figure 3.26. Contact angle measurement of Cu ink before and after silanization of F:SnO ₂ /glass, respectively.....	47
Figure 3.27. Contact angle measurement of Co ink before and after silanization of F:SnO ₂ /glass, respectively.....	48
Figure 3.28. Contact angle measurement of Fe ink before and after silanization of F:SnO ₂ /glass, respectively.....	48
Figure 3.29. Contact angle measurement of Cr ink before and after silanization of F:SnO ₂ /glass, respectively.....	49
Figure 3.30. a) Precision of cyclic voltammograms for printed NiO catalyst in 1 M KOH electrolyte with a scan rate of 100mV/s b) Chronoamperometry of printed NiO catalyst in 1 M KOH electrolyte c) Sequentially printed NiO catalysts before cyclic voltammetry measurement d), e) Optical microscopic image with different magnifications printed NiO catalyst f) Sequentially printed NiO catalysts after cyclic voltammetry measurement.....	51

<u>Figure</u>	<u>Page</u>
Figure 3.31. a) Precision of cyclic voltammograms for printed Mn ₃ O ₄ catalyst in 1 M KOH electrolyte with a scan rate of 100mV/s b) Chronoamperometry of printed Mn ₃ O ₄ catalyst in 1 M KOH electrolyte c) Sequentially printed Mn ₃ O ₄ catalysts before cyclic voltammetry measurement d), e) Optical microscopic image with different magnifications printed Mn ₃ O ₄ catalyst f) Sequentially printed Mn ₃ O ₄ catalysts after cyclic voltammetry measurement.....	52
Figure 3.32. a) Precision of cyclic voltammograms for printed Cr ₂ O ₃ catalyst in 1 M KOH electrolyte with a scan rate of 100mV/s b) Chronoamperometry of printed Cr ₂ O ₃ catalyst in 1 M KOH electrolyte c) Sequentially printed Cr ₂ O ₃ catalysts before cyclic voltammetry measurement d), e) Optical microscopic image with different magnifications printed Cr ₂ O ₃ catalyst f) Sequentially printed Cr ₂ O ₃ catalysts after cyclic voltammetry measurement.....	53

LIST OF TABLES

<u>Table</u>	<u>Page</u>
Table 1.1. Overpotential (η) values of state-of-the-art OER and HER catalysts under acidic and alkaline conditions (McCrorry 2015).....	4
Table 2.1. Surface tension measurements of catalyst precursor inks.....	9
Table 2.2. Viscosity measurements of catalyst precursor inks.....	10
Table 2.3. Proportionally calculated volume of evaporated sample and molarity change in container.....	18
Table 3.1. Tafel slopes for Pt wire in 1 M KOH electrolyte (1 M NaOH electrolyte in the literature).....	24
Table 3.2. Tafel slopes for Ni foam in 1 M KOH electrolyte (1 M NaOH electrolyte in the literature).....	25
Table 3.3. Tafel slopes for IrO ₂ in 1 M KOH electrolyte.....	26
Table 3.4. Overpotential measurements for printed NiO, Mn ₃ O ₄ and Cr ₂ O ₃ catalyst samples.....	31
Table 3.5. Overpotential measurements for printed Ni _{0.85} Fe _{0.1} Co _{0.05} O _x , Ni _{0.45} Fe _{0.15} Co _{0.4} O _x and Ni _{0.15} Fe _{0.35} Co _{0.5} O _x catalyst samples.....	36
Table 3.6. Water oxidation overpotential measurements for printed Ni _x Co _y Cu _z O _n catalyst samples @ 10 mA/cm ²	39
Table 3.7. Appropriate co-solvents and related properties.....	44
Table 3.8. Contact angle measurements for pure water and printer inks.....	49
Table 3.9. Overpotential measurements for bare F:SnO ₂ /glass and drop casted NiO, Mn ₃ O ₄ and Cr ₂ O ₃ catalyst samples.....	54

CHAPTER 1

INTRODUCTION

1.1. Global Energy Supply Problem

Nowadays, as we experience a global disaster caused by the COVID-19 outbreak which could radically modify our lifestyle and habits, the interest in the scientific solutions is gradually increasing worldwide. In many respects this situation is like a rehearsal of the challenges that the climate crisis will bring.

The aim to prevent the upcoming climate crisis is to remain below the 2 °C temperature increase compared to the pre-industrial period. It is envisaged to achieve this goal by reducing the CO₂ emission that constitutes 2/3 of the greenhouse gases (IRENA 2019).

Global power consumption of population is expected to be 30 TW by 2050s (Van de Krol 2012). Fossil fuels which has the largest share in today's energy supply are limited to a few centuries at most and causes severe environmental problems by increasing the CO₂ emissions. Distribution of the global energy consumption is dependent 41% on petroleum, 20% on natural gas, 18% on electricity, 16% on coal and only 4% on renewable energy sources as of 2019 (Administration 2019).

Renewable energy production emerges from this need and recent improvements are aiming to reduce costs of renewable energy supplies such as photovoltaic and wind energy.

1.2. Global Energy Storage Problem

The main problem of renewable energy supply is the chaotic nature of the sources which should only be overcome by storing the captured energy.

In comparison to conventional storage technologies like batteries or mechanical and gravitational force driven storage, fuels derived by renewable sources show

superiority by means of high energy storage densities and their ability to be easily transported. As a fuel hydrogen has the highest gravimetric energy density of 143 MJ/kg where coal (24 MJ/kg), gasoline (44 MJ/kg), diesel (46 MJ/kg) and natural gas (54 MJ/kg) stay far behind (Van de Krol 2012). Increasing growth of H₂ research recently is due to the rapid decrease in the cost of H₂ from renewables and the shift from the auto industry to energy-intensive industries like trucks, aviation, shipping and heating applications (Agency 2019).

1.3. Artificial Photosynthesis

Photosynthesis is a biologically catalyzed energy supply reaction which evolution optimized for years with a success which cannot be imitated yet. It is briefly the solar radiated conversion of CO₂ and H₂O into oxygen and glucose which is the chemical fuel for the plant.

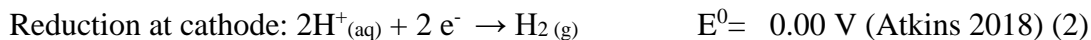
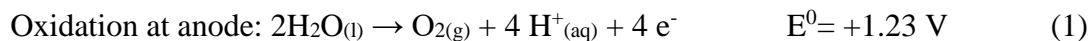
The reasons mentioned above makes the idea of simulating this natural phenomena very attractive in recent years. Artificial photosynthesis is simply deriving fuels from a renewable source. Fuels studied by means of artificial photosynthesis are basically H₂ by water splitting, alcohols/other organic fuels derived from CO₂, NH₃ via Haber-Bosch process.

Topics focused on artificial photosynthesis are the search of absorbers that absorb at the appropriate wavelength and highly efficient catalysts to prevent losses and degradations at the interface of the components that make up the electrochemical system (Montoya et al. 2017).

1.4. Water Splitting

Hydrogen is at the heart of the energy and food supply as it is a building block for both fuels and fertilizers. Since water is the most abundant source, electrolysis will be the key to sustainable production of hydrogen which is the most conventional process for water splitting. Moreover, studies about the OER and HER systems are much more numerous since they are less complex than the CO₂RR.

Following are the half-cell reactions for water splitting:



OER is the rate-determining step involving $4e^-$ transfers. Thus most research studies including this thesis study focus on this half reaction. The band gap required for photoelectrochemical oxidation of water was determined as 1.9-3.1 eV (400-650 nm). The lower limit was calculated by taking into account the energy required for water splitting (1.23 eV), thermodynamic losses (0.3-0.4 eV) and altering reaction kinetics to a feasible level (0.4-0.6 eV) and the upper limit was found by considering the 400 nm wavelength at which the sunlight intensity started to drop rapidly (Van de Krol 2012).

The photoelectrochemical splitting of water was first carried out in the 1970s using n-TiO₂ electrodes (Fujishima 1972). Subsequently p-CdTe, p-GaP, n-TiO₂, n-SrTiO₃ (Ohashi 1977), p-InP (Heller 1982), p-GaInP₂ (Khaselev 1998) were utilized in laboratory-scale.

Sustainable electrolysis of water techniques vary depending on whether the light source is used directly (photoelectrolysis) or indirectly as renewable source (photovoltaics or wind energy) coupled electrolysis. Photoelectrolysis is advantageous over renewable source coupled electrolysis since it is cheaper than the coupled device depending on the auxiliary equipment costs, better heat management since the electrolyte cools the electrode and temperature increase alters the reaction rate approximately by a factor of 2 per 10°C increase as stated in Arrhenius' Law, it causes less gas bubbles resulting in smaller loss in the electrochemically active electrode area. On the other hand it also has disadvantages like the need for semiconductors which is corrosion resistant and having a suitable band gap for photoelectrochemical water splitting (1.9-3.1 eV) and long carrier lifetimes for tandem or single component photoelectrodes, scaling-up these devices introduces mass transfer limitations and standardization studies are needed to be made in order to obtain universality in experiments (Van de Krol 2017).

1.5. State of the Art Catalysts for OER and HER

Requirements for a good catalyst is suitable band gap and band edge positions, donor/acceptor density, carrier lifetime, conductivity, stability and cost.

The current density of $10 \text{ mA/cm}^2_{(\text{geometric area})}$ corresponds to 10% solar to hydrogen efficiency in the presence of 1 sun intensity (McCrorry et al. 2015). In this study, overpotential values corresponding to $10 \text{ mA/cm}^2_{(\text{geometric area})}$ current density are considered as catalyst descriptors.

Although there are electrocatalysts that has low overpotentials in both acidic and basic environment for HER, OER electrocatalysts that are efficient without a tendency for corrosion in acidic electrolyte systems are limited to several precious metals but the number of OER electrocatalysts that has low overpotentials in the basic environment are quite high. Therefore this study is focused on the OER electrocatalysts working in alkaline medium. Examining Table 1.1, general trend is towards alloys of metal catalysts due to the limited yields that can be obtained with a single metal catalyst.

Table 1.1. Overpotential (η) values of state-of-the-art OER and HER catalysts under acidic and alkaline conditions (McCrorry 2015)

OER Catalysts				HER Catalysts			
Acidic Electrolysis	η (mV)	Alkaline Electrolysis	η (mV)	Acidic Electrolysis	η (mV)	Alkaline Electrolysis	η (mV)
(1 M H_2SO_4)		(1 M NaOH)		(1 M H_2SO_4)		(1 M NaOH)	
NiSn alloy (Santos 1992)	140 ± 10	RuO_2 (Tsuji et al. 2011)	290 ± 30	Pt (Walton 1996)	50 ± 10	Pt (Walton 1996)	30 ± 10
RuO_2 (Tsuji et al. 2011)	280 ± 30	NiFeO_x (Merrill and Dougherty 2008)	340 ± 20	NiW alloy (Raj 1990)	60 ± 20	NiW alloy (Raj 1990)	200 ± 30

(cont. on next page)

Table 1.1 (cont.)

OER Catalysts				HER Catalysts			
Acidic Electrolysis		Alkaline Electrolysis		Acidic Electrolysis		Alkaline Electrolysis	
(1 M H ₂ SO ₄)	η (mV)	(1 M NaOH)	η (mV)	(1 M H ₂ SO ₄)	η (mV)	(1 M NaOH)	η (mV)
IrO ₂ (Spurgeon, Velazquez, and McDowell 2014)	340 ± 10	NiMoFe composite (Jayalakshmi 2008)	340 ± 20	NiSn (Yamashita 1993)	390 ± 90	NiMoFe codeposit (Raj 1992)	130 ± 20
		CoFeO _x (Merrill and Dougherty 2008)	350 ± 10	NiMoFe codeposit (Raj 1992)	90 ± 10	NiMoCo codeposit (Fan 1994a)	70 ± 30
		Ni _{0.2} Co _{0.3} Ce _{0.5} O _x (Haber et al. 2014)	350 ± 10	NiMoCo codeposit (Fan 1994a)	50 ± 10	NiMo codeposit (Fan 1994b)	40 ± 20
		NiZn alloy (Santos 1992)	360 ± 20	NiMo codeposit (Fan 1994b)	45 ± 4	NiFe composite (Solmaz 2009)	90 ± 40
		Ni ₂₀ Co ₈₀ alloy (Ho 1996)	380 ± 10	NiFe composite (Solmaz 2009)	220 ± 60	NiCo alloy (Raj 1990)	210 ± 20
		IrO ₂ (Spurgeon, Velazquez, and McDowell 2014)	390 ± 10	NiCo alloy (Raj 1990)	160 ± 30	Ni (Solmaz 2009)	260 ± 40

(cont. on next page)

Table 1.1 (cont.)

OER Catalysts				HER Catalysts			
Acidic Electrolysis (1 M H ₂ SO ₄)	Alkaline Electrolysis		Acidic Electrolysis (1 M H ₂ SO ₄)	η (mV)	Alkaline Electrolysis (1 M NaOH)	η (mV)	
	η (mV)	(1 M NaOH)					
	NiSn alloy (Santos 1992)	390 ± 10	Ni (Solmaz 2009)	370 ± 40	FeMo alloy (Elezovic 2005)	220 ± 30	
	NiCr(OH) ₂ (Li 2011)	390 ± 20	MoS ₂ (Merki et al. 2011)	220 ± 10	Fe (Solmaz 2009)	130 ± 10	
			FeMo alloy (Elezovic 2005)	230 ± 40	CoW (Fan 1994b)	220 ± 10	
			CoW (Fan 1994b)	180 ± 20	CoNiFe alloy (Jafarian 2007)	250 ± 20	
			CoNiFe alloy (Jafarian et al. 2007)	370 ± 30	CoMo (Fan 1994b)	100 ± 20	
			CoMo (Fan 1994b)	100 ± 20	Co (Savadogo 1992)	220 ± 20	
			Co (Savadogo 1992)	230 ± 30			

Pt is the most efficient electrocatalyst for HER, as IrO₂ and RuO₂ are for OER. Earth-abundant catalysts are investigated for both OER and HER (Van de Krol 2012). Metal oxides are preferred mostly owing to their thermodynamical stabilities. Ni, Mn, Cu, Fe, Cr and Co metals are chosen for this thesis study for their abundance, proven

efficiency, low toxicity and aqueous phase stability which are stated in the literature (Merrill and Dougherty 2008).

1.6. Combinatorial Approach and Inkjet Printing of Catalysts

Combinatorial approach which means synthesizing high numbers of material combinations in parallel, in a short time has a wide impact in medicine and materials science. The first practical comprehensive application of the approach is for drug discovery in the pharmaceutical industry (Terrett et al. 1995). Mallouk group used this approach for electrochemical applications for the first time in 1998 (Reddington et al. 1998). Afterwards it has found many uses in searching electronic, magnetic, optical and catalytic materials.

Inkjet printing is a unique high-throughput technology as it combines speed, consistency and precision both for laboratory scale and industry scale applications among diverse techniques developed for deposition of metal oxides on conductive surfaces (Costa Bassetto et al. 2018).

1.7. Main Scientific Question

This study focuses on the scientific question of “Can we obtain an efficient multi-metal oxide catalyst for OER reaction by high-throughput synthesis using inkjet printing?” Also it is aimed to provide a foresight for scale-up production of (photo)electrocatalysts for water splitting. It plans to investigate the procedure, report the difficulties encountered in this experimental method and develop suggestions to overcome them.

CHAPTER 2

INKS AS CATALYST PRECURSORS FOR INKJET PRINTING

2.1. Materials

Inkjet buffer ink for metal salts were supplied from Sağlık İzleme Sistemleri A.Ş. (SIZ+). Corresponding metal salts were added to conduct experiments. $\text{Ni}(\text{NO}_3)_2 \cdot 6\text{H}_2\text{O}$, $\text{Mn}(\text{NO}_3)_2 \cdot 4\text{H}_2\text{O}$, $\text{Co}(\text{NO}_3)_2 \cdot 6\text{H}_2\text{O}$, $\text{Cu}(\text{NO}_3)_2 \cdot 2.5\text{H}_2\text{O}$, $\text{Fe}(\text{Cl}_3)_3 \cdot 6\text{H}_2\text{O}$, $\text{Cr}(\text{NO}_3)_3 \cdot 9\text{H}_2\text{O}$ and Ethanol (96%) were purchased from Chempure Private Limited, Sigma-Aldrich, Tekkim and Merck. SIZ+ Inkjet Material Printer was supplied from SIZ+ for deposition procedures.

2.2. Characterization of the Inks

2.2.1. Surface Tension

2.2.1.1. Experimental Procedure

Measurements were taken with Krüss K10 ST tensiometer device. Surface tension results are determined by De Noüy ring method and indicated as dyn/cm.



Figure 2.1. The experimental setup for surface tension measurement of precursor inks

2.2.1.2. Results and Discussion

Table 2.1. Surface tension measurements of catalyst precursor inks

	Literature Range (Liu et al. 2012)	Ni	Mn	Cu	Cr	Fe	Co
Surface Tension (dyn/cm)	20 - 55	26.1	27.3	25.9	26.4	27.3	26.4

It has been reported in the literature that surface tension should be in 20 – 55 dyn/cm range for droplet formation in piezoelectric inkjet printers (Liu et al. 2012). It is very important that the surface tension value is close to the lower limit so that the substrate can be wetted optimally. The surfactant used in ink allowed this adjustment.

2.2.2. Viscosity

2.2.2.1. Experimental Procedure

Viscosity measurements were taken with NDJ-1 viscosimeter with a #0 rotor and indicated as cP.



Figure 2.2. The experimental setup for viscosity measurement of precursor inks

2.2.2.2. Results and Discussion

Table 2.2. Viscosity measurements of catalyst precursor inks

	Literature Range (Liu et al. 2012)	Ni	Mn	Cu	Cr	Fe	Co
Viscosity (cP)	5 - 30	4.37	4.34	4.07	4.31	3.86	4.4

High viscosity although being useful to reduce the amount of droplets formed in the nozzle and cause thinner film formation (Sun et al. 2013), it must be low enough to prevent clogging in the inkjet printhead. Therefore measured viscosity values despite being below the literature range for piezoelectric inkjet printing (Liu et al. 2012) were optimized through trial and error to facilitate inkjet printing by SIZ+ Inkjet Material Printer and prevent clogging.

2.2.3. Volatility

2.2.3.1. Experimental Procedure

To test volatility of inks 14 mL of Ni, Mn, Cr, Fe, Co and Cu inks were filled in metered test tubes. At the same time, equivalent volume of Epson T673 ink, ethanol, acetic acid and SIZ+ inkjet buffer ink for metal salts were also filled respectively for comparison:



Figure 2.3. The experimental setup for volatility of precursor inks

2.2.3.2. Results and Discussion

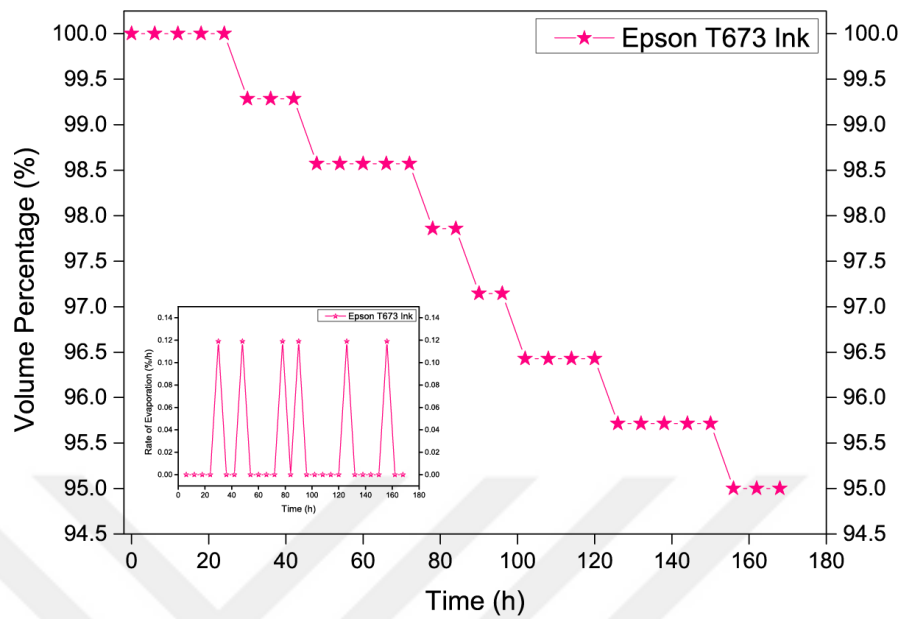


Figure 2.4. The change of percentage due to evaporation for Epson T673 ink with respect To time (0.7 mL out of 14 mL) (inset: evaporation rate)

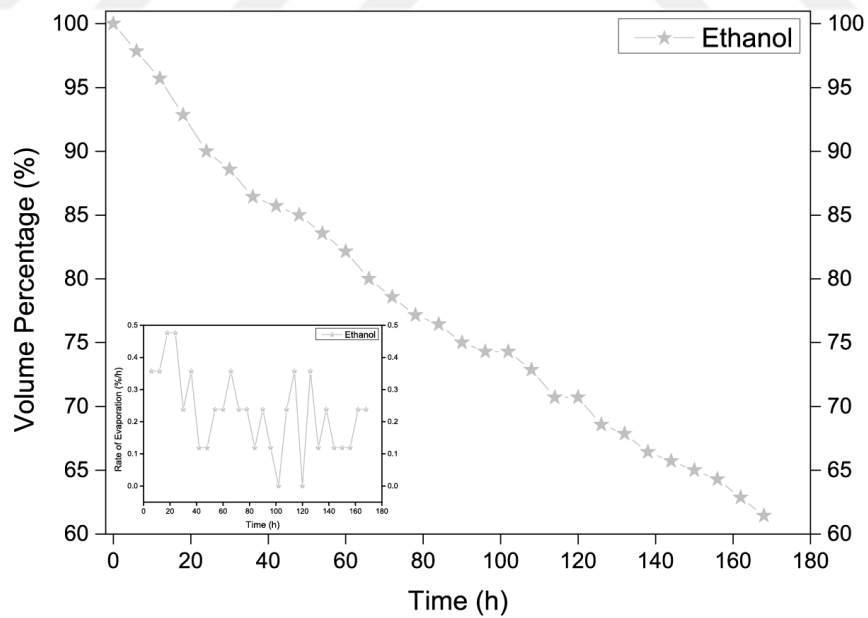


Figure 2.5. The change of percentage due to evaporation for ethanol with respect to time (5.4 mL out of 14 mL) (inset: evaporation rate)

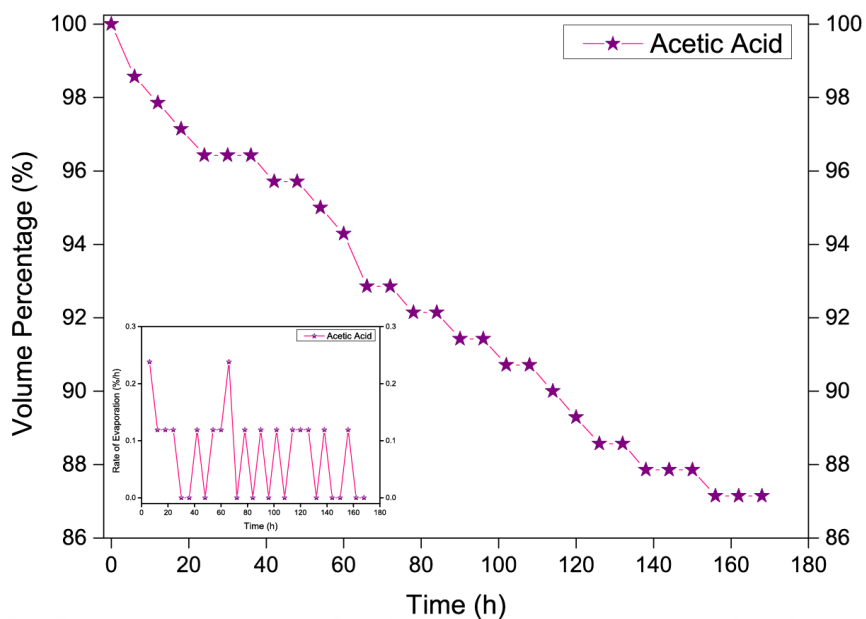


Figure 2.6. The change of percentage due to evaporation for acetic acid with respect to time (1.8 mL out of 14 mL) (inset: evaporation rate)

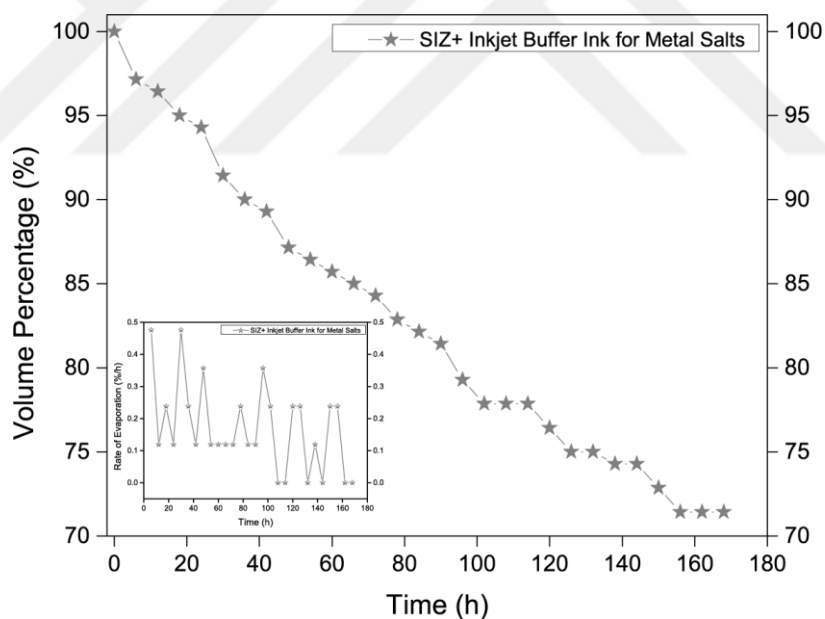


Figure 2.7. The change of percentage due to evaporation for SIZ+ inkjet buffer ink for metal salts with respect to time (4 mL out of 14 mL) (inset: evaporation rate)

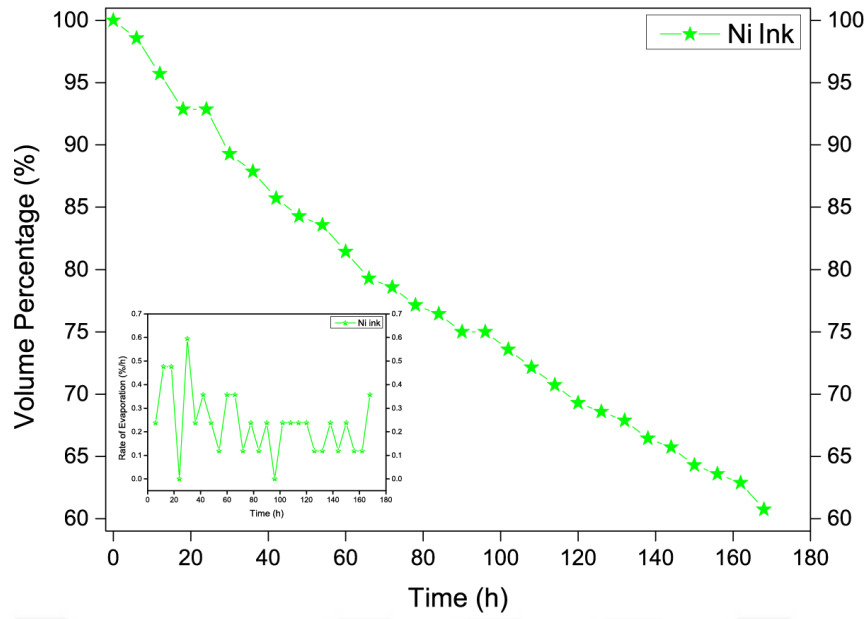


Figure 2.8. The change of percentage due to evaporation for Ni ink with respect to time (5.5 mL out of 14 mL) (inset: evaporation rate)

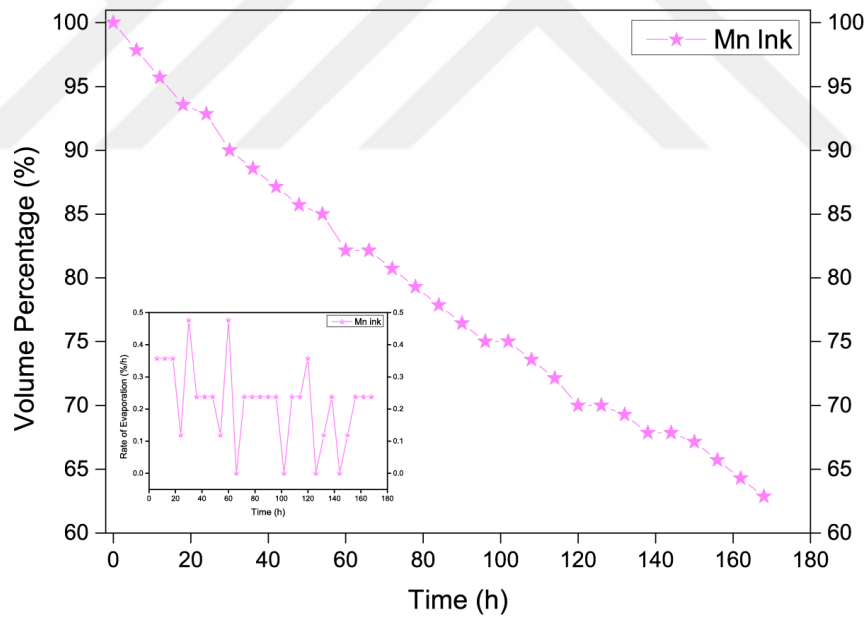


Figure 2.9. The change of percentage due to evaporation for Mn ink with respect to time (5.2 mL out of 14 mL) (inset: evaporation rate)

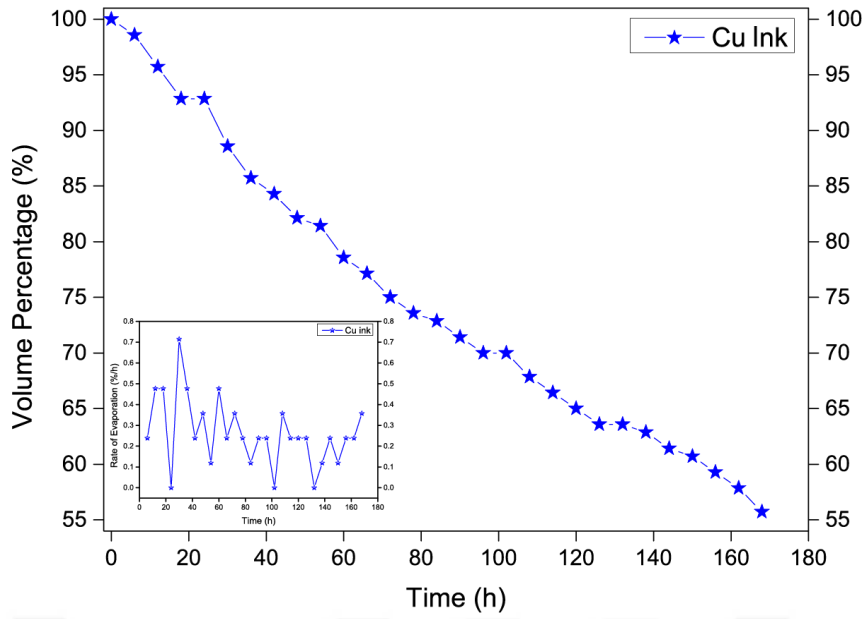


Figure 2.10. The change of percentage due to evaporation for Cu ink with respect to time (6.2 mL out of 14 mL) (inset: evaporation rate)

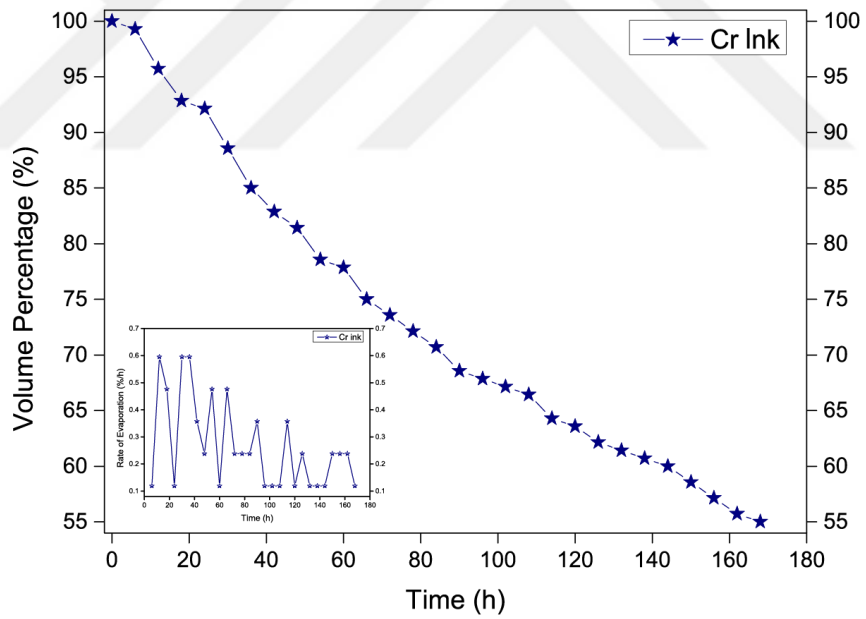


Figure 2.11. The change of percentage due to evaporation for Cr ink with respect to time (6.3 mL out of 14 mL) (inset: evaporation rate)

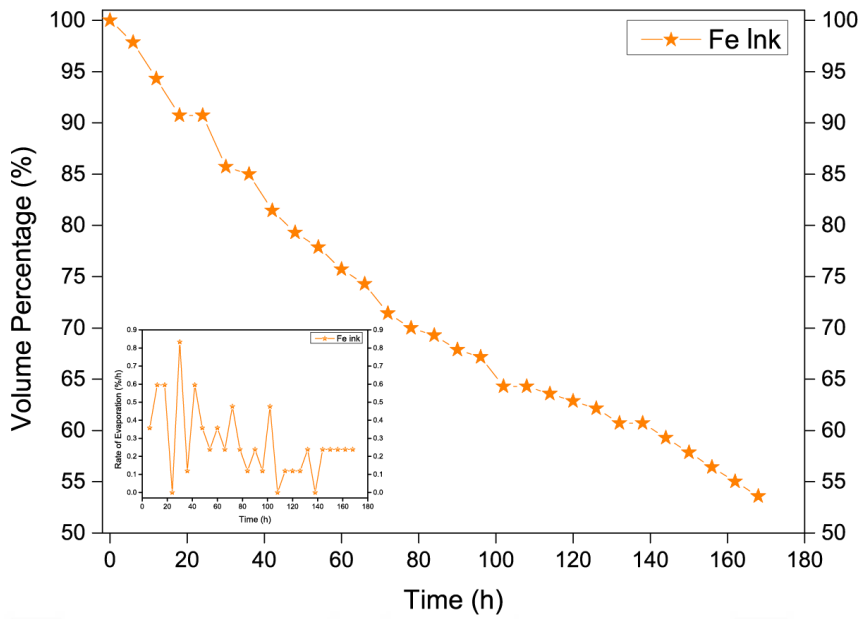


Figure 2.12. The change of percentage due to evaporation for Fe ink with respect to time (6.5 mL out of 14 mL) (inset: evaporation rate)

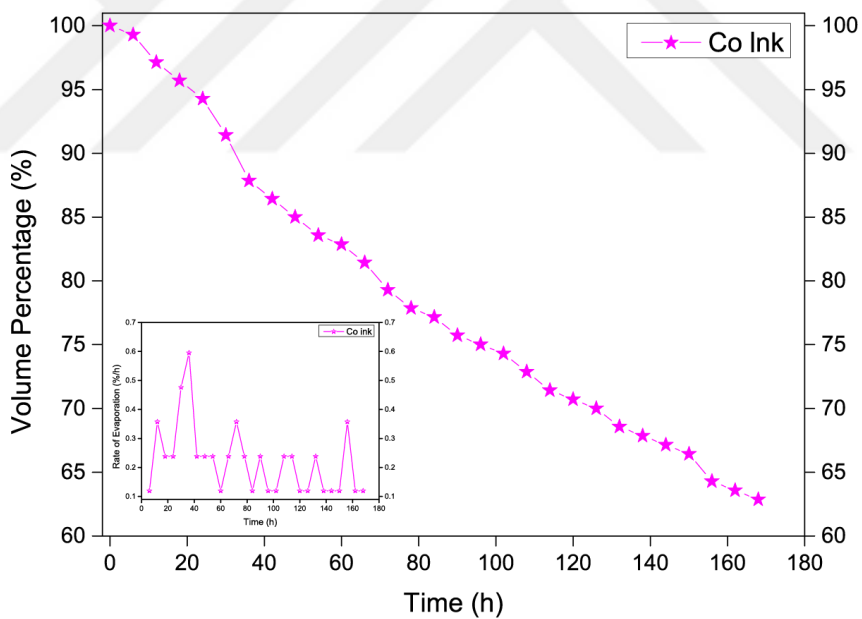


Figure 2.13. The change of percentage due to evaporation for Co ink with respect to time (5.2 mL out of 14 mL) (inset: evaporation rate)

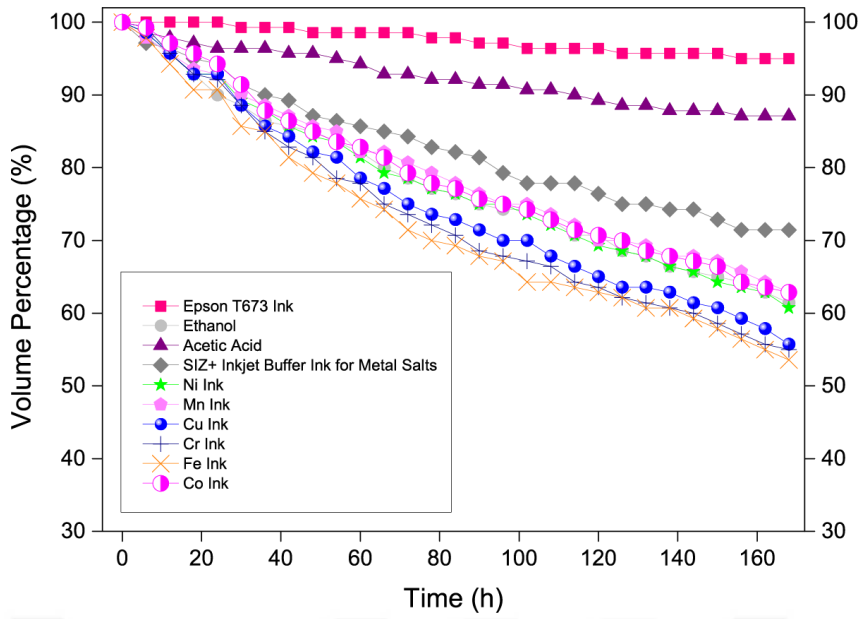


Figure 2.14. The comparison of the change of percentage due to evaporation for all samples with respect to time



Figure 2.15. Dimensions of the ink containers used

Table 2.3. Proportionally calculated volume of evaporated sample and molarity change in container

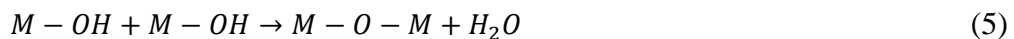
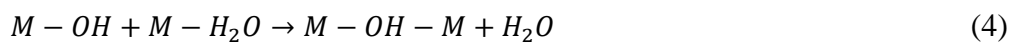
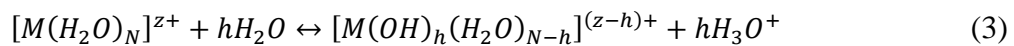
Cross-sectional Area (cm ²)	Total Volume (mL)	Evaporated Volume (mL)				Molarity Change (mol/L)			
		Ni, Co	Mn, Cu	Cr, Fe	Ni, Co	Mn, Cu	Cr, Fe		
8.05	14	5.3	6.3		0.609		0.818		
10	70	6.6	7.8		0.104		0.125		
90x2.83x10⁻⁵	1*	1.68x10 ⁻³	1.99x10 ⁻³		1.68x10 ⁻³		1.99x10 ⁻³		

*Estimated value of each ink reservoir

Ink volatility should be minimized so that the inks do not cause clogging of the inkjet printhead (Martin, Hoath, and Hutchings 2008). It has been observed that if the solvents with a vapor pressure higher than approximately 100 mmHg are used, the droplet loses its stability and does not even allow droplet formation (Zhan et al. 2017). In addition to the viscosity and surface tension, evaporation behaviour plays an important role in optimizing the interaction force between the substrate and the ink in order to make the coated film homogeneous (Kuang, Wang, and Song 2014).

Test results reveal that the inks used in the experiments are more volatile than the components and the Epson T673 ink. On the other hand inks have been shown to be much more cost effective than EPSON T673 ink which makes them suitable for scale-up studies. In order to prevent clogging caused by volatility, a head cleaning procedure with ethanol has been developed after each printing. Possible cause of the volatility is indicated as follows:

Adding metal salts result in formation of aquacations (3) which undergo condensation [olation (4) and oxolation (5)] reactions (Cochran et al. 2019):



Reaction 1 is possibly the reason of increase in acidity in our ink solutions shown in the Figure 2.16. The higher the oxidation number of metal cation, the more H^+ ions release to the solution. Reaction 2 and 3 are the possible reasons for the increase in volatility by adding the metal salts provided they are exothermic.

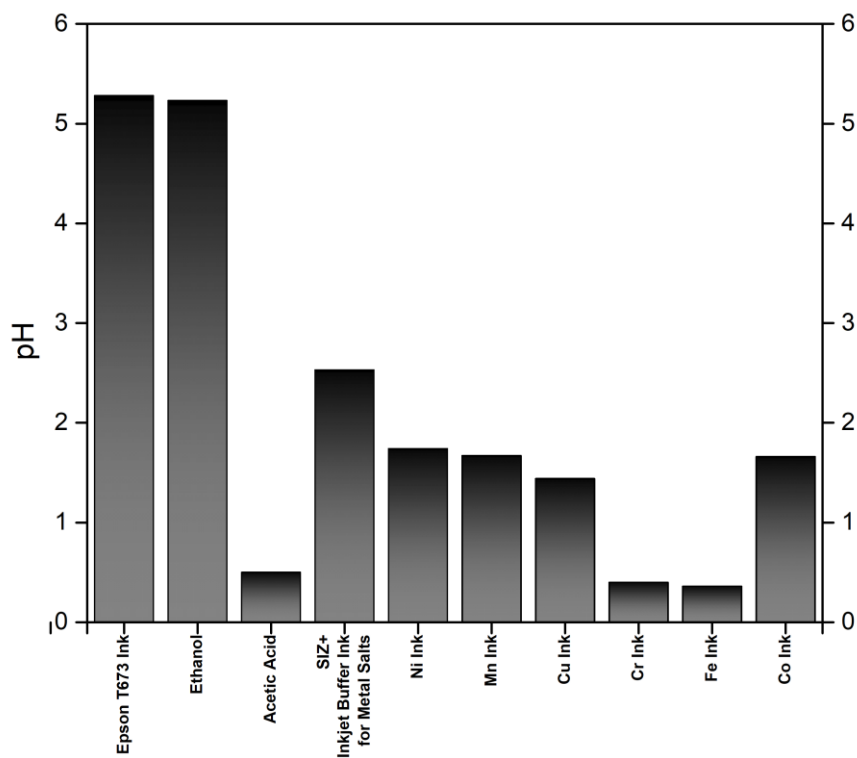


Figure 2.16. pH measurements of tested samples

CHAPTER 3

EXPERIMENTAL VALIDATION

3.1. Printer Test Protocol

3.1.1. Effect of Tray Position

3.1.1.1. Experimental Procedure

As seen in the pictures below distance of the tray from the inkjet printhead affects the quantity of catalyst printed on a specific area. Circular pattern of Co-ink is printed with increasing distance. Increments were set as 2 mm.



Figure 3.1. Measurement of distance between the inkjet printhead and the tray

As analyzed with a VEGA USB2.0 camera, the area of the total circle pattern thus the area of each droplet increases with increasing distance. Since the total amount of catalyst remains the same, boundaries tend to be less clear.

3.1.1.2. Results and Discussion

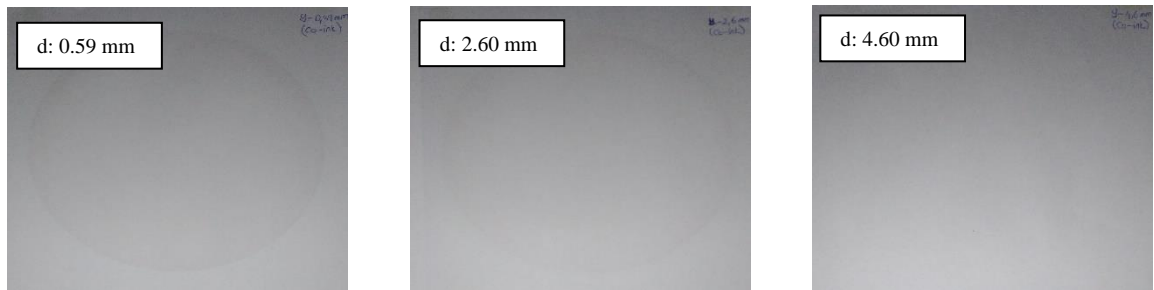


Figure 3.2. Printed circular patterns with increasing distances

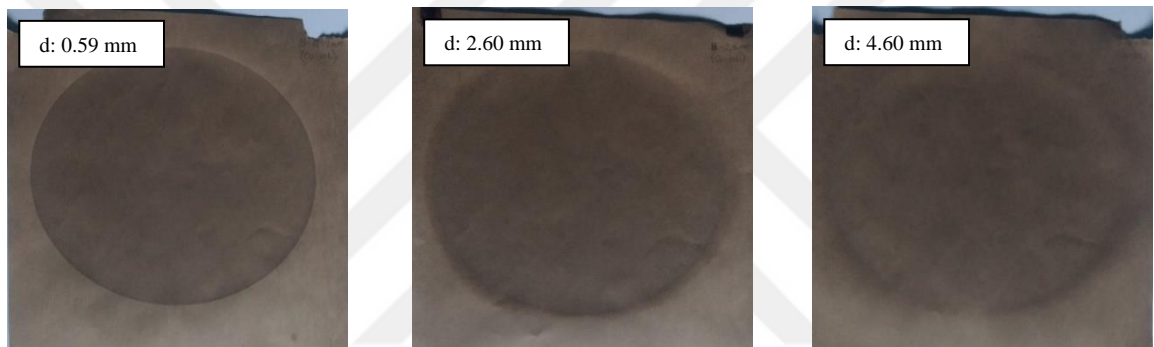


Figure 3.3. Printed circular patterns with increasing distances after oxidation at 230 °C for 60 minutes

Procedure confirmed that resolution increases with decreasing distance between the inkjet printhead and the tray which indicates that the smaller the distance, the greater the quantity of catalyst per printed area. For this reason, the distance between the substrate and the inkjet printhead was kept constant at 0.6 mm for the prints taken during the experiment.

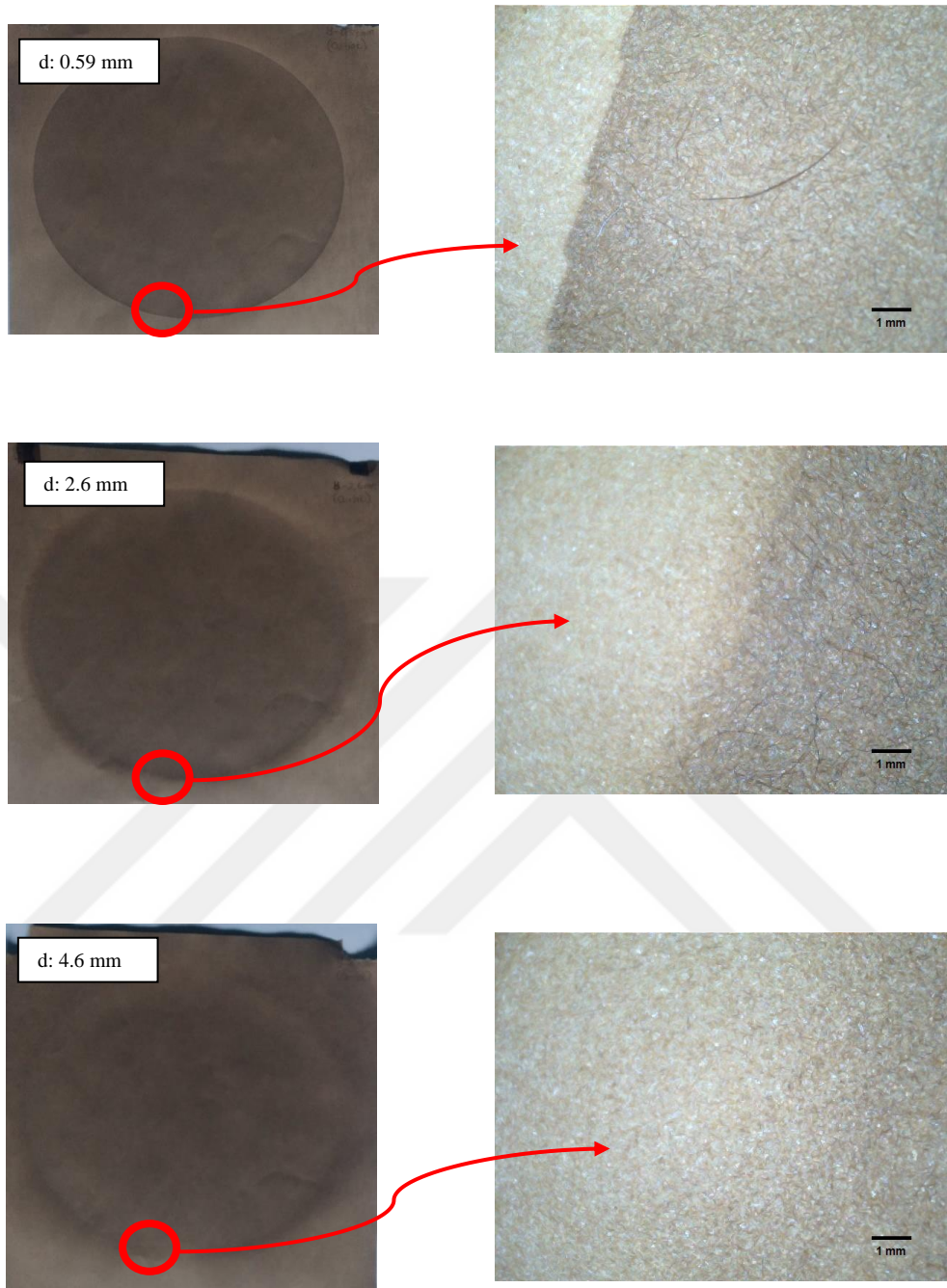


Figure 3.4. Optical microscopy images for examination of the boundaries

3.1.2. Precision & Accuracy Test

3.1.2.1. Electrocatalyst Measurement Protocol

3.1.2.1.1. Experimental Procedure

Pt wire, Ni foam and IrO₂ were electrochemically characterized and corresponding Tafel plots were derived from cyclic voltammetry and chronopotentiometry data. Electrochemical measurements were taken using CV in a three-electrode system with an Autolab PGSTAT204 potentiostat. Ag/AgCl was used as the reference electrode and Pt mesh was used as the counter electrode where Pt wire, Ni foam and IrO₂ were employed as the working electrodes, respectively. As the electrolyte, 1 M KOH was used for all of the catalysts with varying scan rates. Current densities were measured against the voltage vs RHE, which is calculated considering the theoretical pH of the electrolyte (pH=14 for 1 M KOH) according to the formula:

$$E_{\text{RHE}} = E_{\text{measured}} + E_{\text{Ag/AgCl}} + 0.059 \cdot \text{pH} \quad (6)$$

($E_{\text{Ag/AgCl}} = 0.205 \text{ V}$ for electrode stored in 3.5 M KCl)

Onset potentials in cyclic voltammograms of Pt wire 1.63 V (Ranaweera et al. 2017), Ni foam 1.56 V (Ranaweera et al. 2017), and IrO₂ 1.48 V (Qin et al. 2018), being similar to the literature, their Tafel slopes indicated differences with the literature values. The factors affecting the slopes may be multiple.

Since the current densities are normalized by the geometric area of the catalyst it is suggested that underlying reason for these inconsistencies was the dissimilar catalyst loading between the experimental procedure and the literature. Although IrO₂ was stated 1.6 mg/cm² in the literature, information about the loadings of Pt and Ni foam is insufficient.

Also electrochemical cells and electrode positions are also not standard and vary between different research groups which leads to measurement differences and iR compensation % is depending on the equipment used. In the Autolab PGSTAT204 potentiostat setup we use in our experiments maximum iR compensation value is 90% although its upper limit is determined by the fluctuating working electrode potential in the positive feedback for each catalyst, separately.

3.1.2.1.2. Results and Discussion

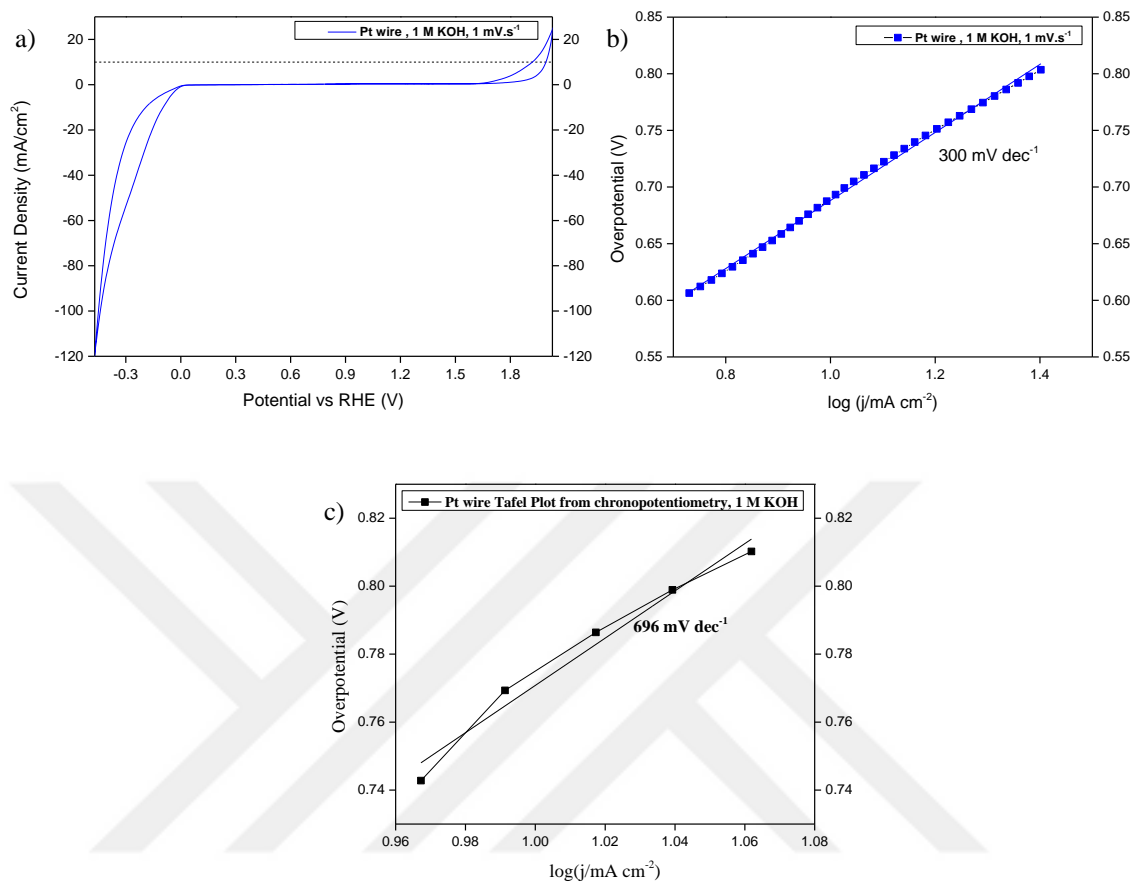


Figure 3.5. a) Cyclic voltammograms for Pt wire in 1 M KOH electrolyte with a scan rate of 1 mV/s, b) Tafel plots derived from cyclic voltammograms for Pt wire in 1 M KOH electrolyte with a scan rate of 1 mV/s, c) Tafel plot derived from chronopotentiometry for Pt wire in 1 M KOH electrolyte

Table 3.1. Tafel slopes for Pt wire in 1 M KOH electrolyte (1 M NaOH electrolyte in the literature)

	Tafel Slope Calculated from CV, (mV dec ⁻¹)	Tafel Slope Calculated from CP, (mV dec ⁻¹)	Tafel Slope in Literature, (mV dec ⁻¹)
	(scan rate 1 mV/s)		(scan rate 1 mV/s)
	(btw 5.5 – 30 mA/cm ²)	300	696
			220 (Ranaweera et al. 2017)

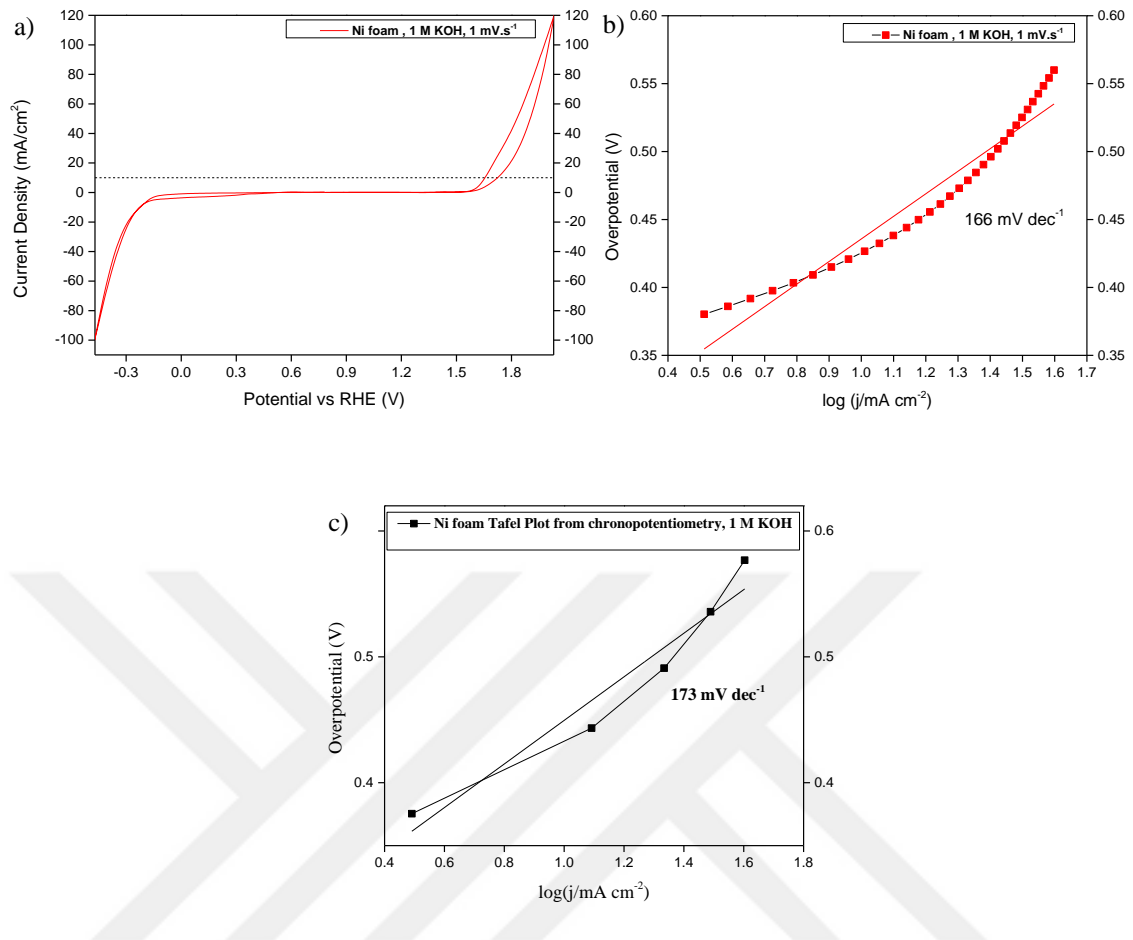


Figure 3.6. a) Cyclic voltammograms for Ni foam in 1 M KOH electrolyte with a scan rate of 1 mV/s, b) Tafel plots derived from cyclic voltammograms for Ni foam in 1 M KOH electrolyte with a scan rate of 1 mV/s, c) Tafel plot derived from chronopotentiometry for Ni foam in 1 M KOH electrolyte

Table 3.2. Tafel slopes for Ni foam in 1 M KOH electrolyte (1 M NaOH electrolyte in the literature)

	Tafel Slope Calculated from CV, (mV dec ⁻¹)	Tafel Slope Calculated from CP, (mV dec ⁻¹)	Tafel Slope in Literature, (mV dec ⁻¹)
	(scan rate 1 mV/s)		(scan rate 1 mV/s)
(btw 3 – 40 mA/cm ²)	166	173	142 (Ranaweera et al. 2017)

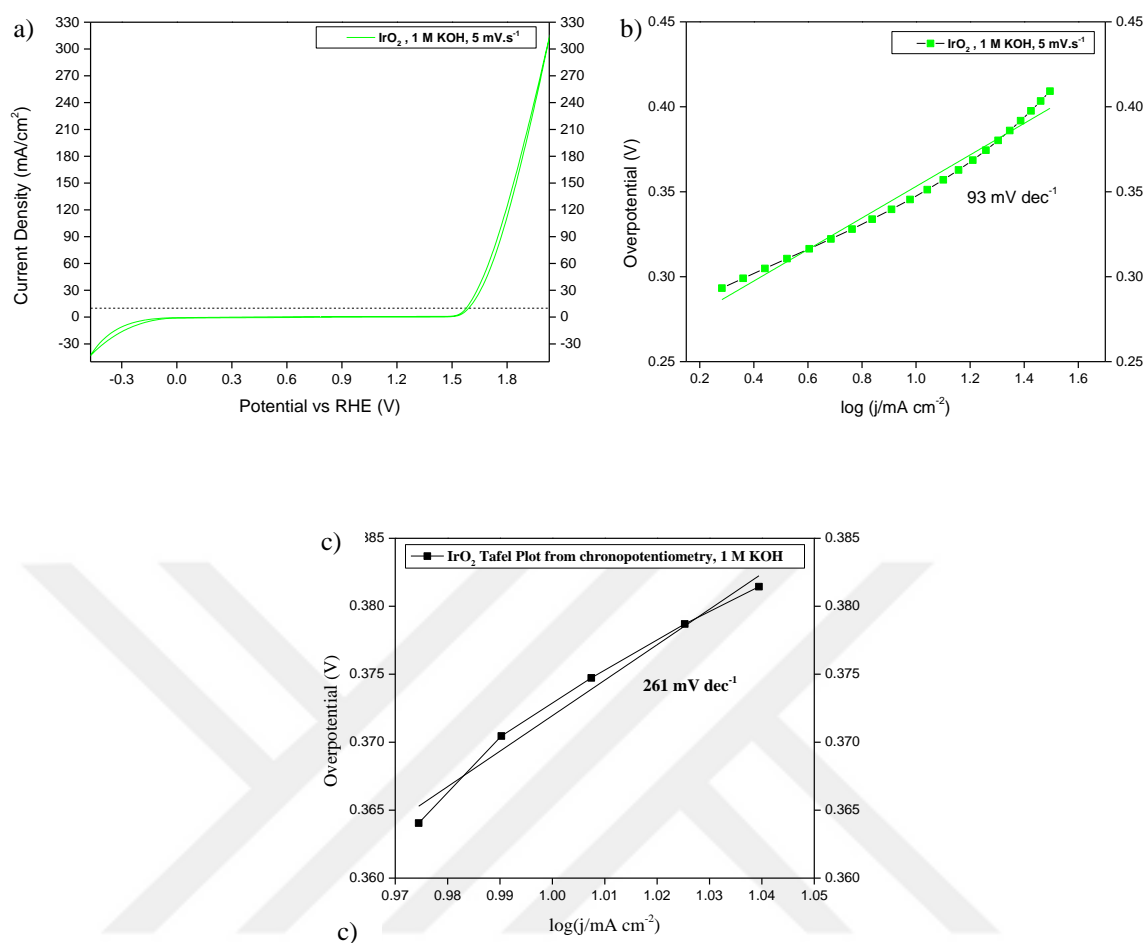


Figure 3.7. a) Cyclic voltammograms for IrO₂ in 1 M KOH electrolyte with a scan rate of 5 mV/s, b) Tafel plots derived from cyclic voltammograms for IrO₂ in 1 M KOH electrolyte with a scan rate of 5 mV/s, c) Tafel plot derived from chronopotentiometry for IrO₂ in 1 M KOH electrolyte

Table 3.3. Tafel slopes for IrO₂ in 1 M KOH electrolyte

	Tafel Slope Calculated from CV, (mV dec ⁻¹)	Tafel Slope Calculated from CP, (mV dec ⁻¹)	Tafel Slope in Literature, (mV dec ⁻¹)
	(scan rate 5 mV/s)		(scan rate 5 mV/s)
(btw 1.78 – 31.62 mA/cm ²)	93	261	62 (Qin et al. 2018)

Since RHE potential is pH-dependent according to Nernst equation, another reason may be the difference between the theoretical and practical pH value. Literature consists of varying pH values and recently a study was conducted on the differences that may occur (Niu et al. 2020).

One last consideration indicates that inconsistencies may result from different counter electrode areas as the counter electrode used for Pt wire, Ni foam experiments in literature was reported to be Pt wire but the dimensions were not stated in the literature.

3.1.2.2. Single Metal Oxides

3.1.2.2.1. Experimental Procedure

NiO, Mn₃O₄, Cr₂O₃, Co₃O₄, CuO and Fe₂O₃ catalysts were printed with SIZ+ Inkjet Material Printer. To test precision, samples were printed for each catalyst, calcined at 40°C for 18 h, at 70°C for 24 h, at 350°C for 10 h, respectively as reported in the literature (Xiang et al. 2014).

Electrochemical measurements were taken using CV in a three-electrode system with an Autolab PGSTAT204 potentiostat. Ag/AgCl was used as the reference electrode and Pt mesh was used as the counter electrode while catalysts printed on a F:SnO₂/glass were employed as the working electrodes. As the electrolyte, 1 M KOH was used for all of the catalysts with a scan rate of 100 mV/s. Current densities were measured against the voltage vs RHE, which is calculated considering the measured pH of the electrolyte (pH=13 for 1 M KOH) according to the formula:

$$E_{\text{RHE}} = E_{\text{measured}} + E_{\text{Ag/AgCl}} + 0.059 \cdot \text{pH} \quad (6)$$

($E_{\text{Ag/AgCl}} = 0.205$ V for electrode stored in 3.5 M KCl)

For photoelectrochemical measurements, AM 1.5 light source was applied from the back surface of the catalysts.

3.1.2.2.2. Results and Discussion

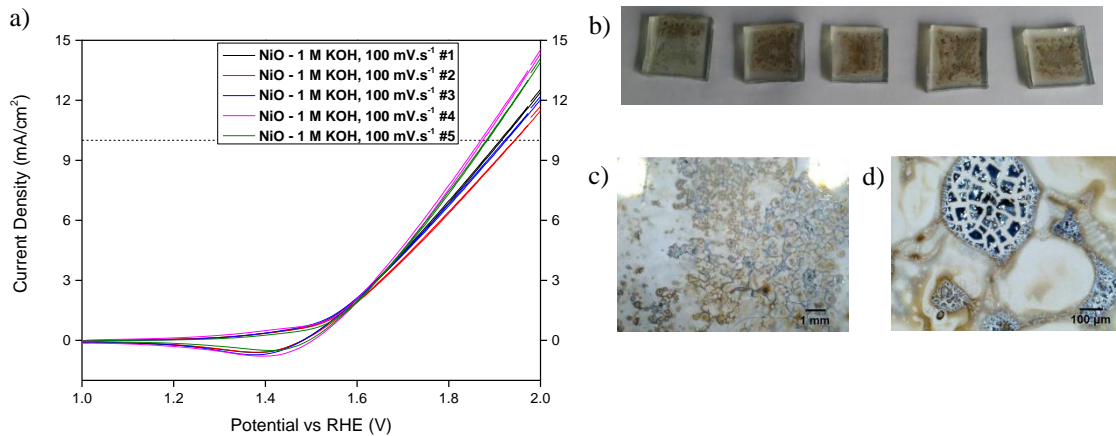


Figure 3.8. a) Precision of cyclic voltammograms for printed NiO catalysts
b) Sequentially printed NiO catalysts c), d) Optical microscopic image with different magnifications printed NiO catalyst

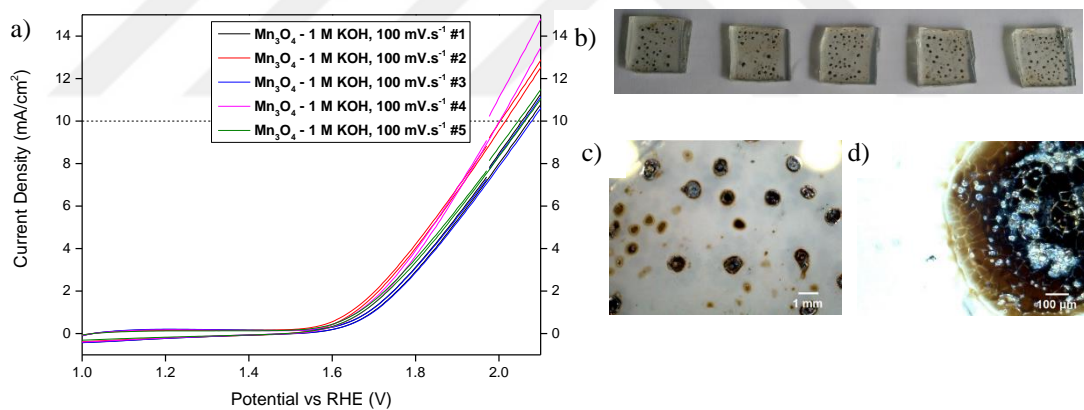


Figure 3.9. a) Precision of cyclic voltammograms for printed Mn₃O₄ catalysts
b) Sequentially printed Mn₃O₄ catalysts c), d) Optical microscopic image with different magnifications printed Mn₃O₄ catalyst

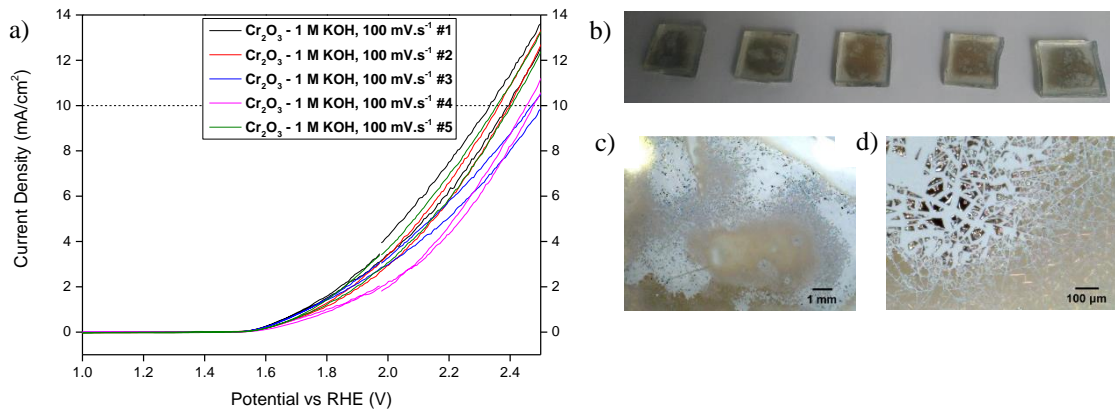


Figure 3.10. a) Precision of cyclic voltammograms for printed Cr₂O₃ catalysts
 b) Sequentially printed Cr₂O₃ catalysts c), d) Optical microscopic image with different magnifications printed Cr₂O₃ catalyst

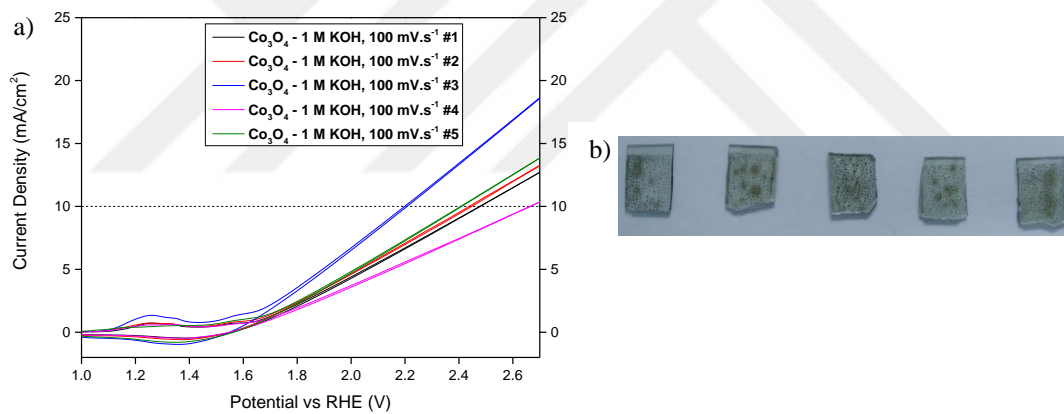


Figure 3.11. a) Precision of cyclic voltammograms for printed Co₃O₄ catalysts
 b) Sequentially printed Co₃O₄ catalysts

Overpotentials (η) given in the table below were calculated by the following formula:

$$\eta = E_{\text{measured}} - 1.23 \quad (7)$$

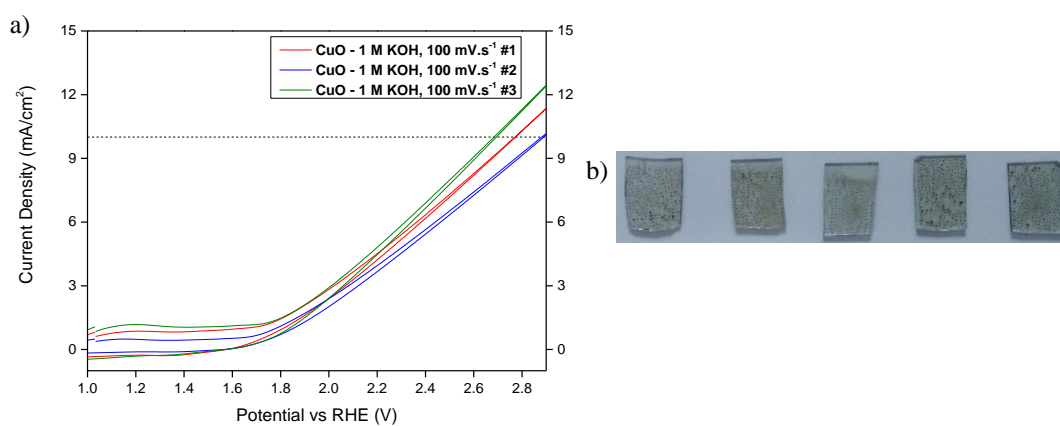


Figure 3.12. a) Precision of cyclic voltammograms for printed CuO catalysts
b) Sequentially printed CuO catalysts

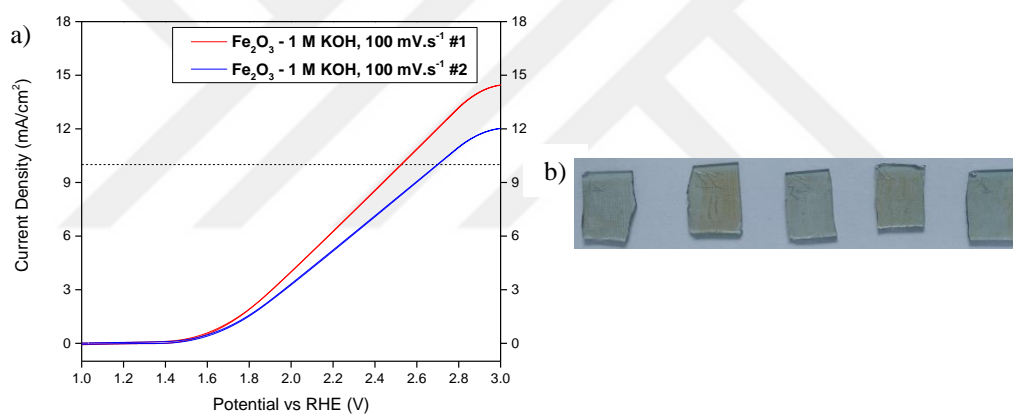


Figure 3.13. a) Precision of cyclic voltammograms for printed Fe₂O₃ catalysts
b) Sequentially printed Fe₂O₃ catalysts

All the deposited metal oxide catalysts partially detached from the F:SnO₂/glass surface and precipitated at the bottom of the cell during electrochemical experiments.

Table 3.4. Overpotential measurements for printed NiO, Mn₃O₄, Cr₂O₃, Co₃O₄, CuO and Fe₂O₃ catalyst samples

Catalyst #	Overpotential Measured, (mV) (@10 mA/cm²)	Overpotential in Article, (mV) (@10 mA/cm²)
NiO - #1	684	420 (McCroory et al. 2013)
NiO - #2	714	
NiO - #3	696	
NiO - #4	644	
NiO - #5	656	
Average	678.8	
Standard Deviation	28.69	
Standard Deviation %	4.23	
	(@10 mA/cm²)	(@10 mA/cm²)
Mn ₃ O ₄ - #1	827	570 (Ramírez et al. 2014)
Mn ₃ O ₄ - #2	774	
Mn ₃ O ₄ - #3	834	
Mn ₃ O ₄ - #4	775	
Mn ₃ O ₄ - #5	821	
Average	806.2	
Standard Deviation	29.3	
Standard Deviation %	3.63	
	(@10 mA/cm²)	
Cr ₂ O ₃ - #1	1108	-
Cr ₂ O ₃ - #2	1137	
Cr ₂ O ₃ - #3	1247	
Cr ₂ O ₃ - #4	1223	
Cr ₂ O ₃ - #5	1131	
Average	1169.2	
Standard Deviation	61.62	
Standard Deviation %	5.27	
	(@10 mA/cm²)	(@10 mA/cm²)
Co ₃ O ₄ - #1	906	429 (Ramírez 2014)

(cont. on next page)

Table 3.4 (cont.)

Co ₃ O ₄ - #2	1176	
Co ₃ O ₄ - #3	1207	
Co ₃ O ₄ - #4	1246	
Co ₃ O ₄ - #5	1434	
Average	1193.8	
Standard Deviation	189.56	
Standard Deviation %	15.88	
	(@10 mA/cm²)	(@10 mA/cm²)
CuO - #1	1454	
CuO - #2	1539	
CuO - #3	1652	475 (Liu et al. 2016)
Average	1548.3	
Standard Deviation	99.33	
Standard Deviation %	6.42	
	Onset	Onset
Fe ₂ O ₃ - #1	248	
Fe ₂ O ₃ - #2	284	420 (Gahlawat, Rashid, and Ingole 2018)
Average	266	
Standard Deviation	25.46	
Standard Deviation %	9.57	

Also, for Cr₂O₃ catalyst no literature for overpotential measurements was found up to date. Besides, the standard deviation of overpotential for Mn₃O₄ catalyst (3.63%) was lowest among all the tested catalysts. The second lowest was NiO catalyst with a standard deviation of 4.23% and the highest standard deviation value belonged to Co₂O₄ catalyst (15.88%). It is suggested that the variation in the standard deviation values is related to thin film properties such as homogeneity of each catalyst. As noticed in the microscope images film homogeneity is an important issue in achieving both higher efficiencies and lower standard deviations. Mn₃O₄ tended to aggregate more than other deposited catalysts.

3.1.2.3. Multi Metal Oxides

3.1.2.3.1. Compositional Scan of Nickel, Iron and Cobalt Oxides

3.1.2.3.1.1. Experimental Procedure

Varying compositions of NiO, Fe₂O₃ and Co₃O₄ catalysts were printed with SIZ+ Inkjet Material Printer. To test precision, 5 samples were printed for each catalyst calcined at 40°C for 18 h, at 70°C for 24 h, at 350°C for 10 h, respectively. Inkjet printed samples analyzed (1, 2 and 3) were chosen according to Fig. 4b of the related article (Xiang et al. 2014).

To test precision, 5 samples were printed for each catalyst calcined at 40°C for 18 h, at 70°C for 24 h, at 350°C for 10 h, respectively.

Electrochemical measurements were taken using CV in a three-electrode system with an Autolab PGSTAT204 potentiostat. Ag/AgCl was used as the reference electrode and Pt mesh was used as the counter electrode while catalysts printed on a F:SnO₂/glass were employed as the working electrodes. 0.1 M NaOH electrolyte was used for all of the measurements with a scan rate of 100 mV/s. Measured current densities were calculated considering the pH of the electrolyte (0.1 M NaOH, pH=11.6) according to the formula:

$$E_{\text{RHE}} = E_{\text{measured}} + E_{\text{Ag/AgCl}} + 0.059 \cdot \text{pH} \quad (6)$$

Average overpotential value of the Ni_{0.85}Fe_{0.1}Co_{0.05}O_x catalyst was consistent with the literature with a standard deviation of 9.77%. There were clear differences between the Ni_{0.45}Fe_{0.15}Co_{0.4}O_x and the Ni_{0.15}Fe_{0.35}Co_{0.5}O_x catalyst's overpotential values and the values in the article.

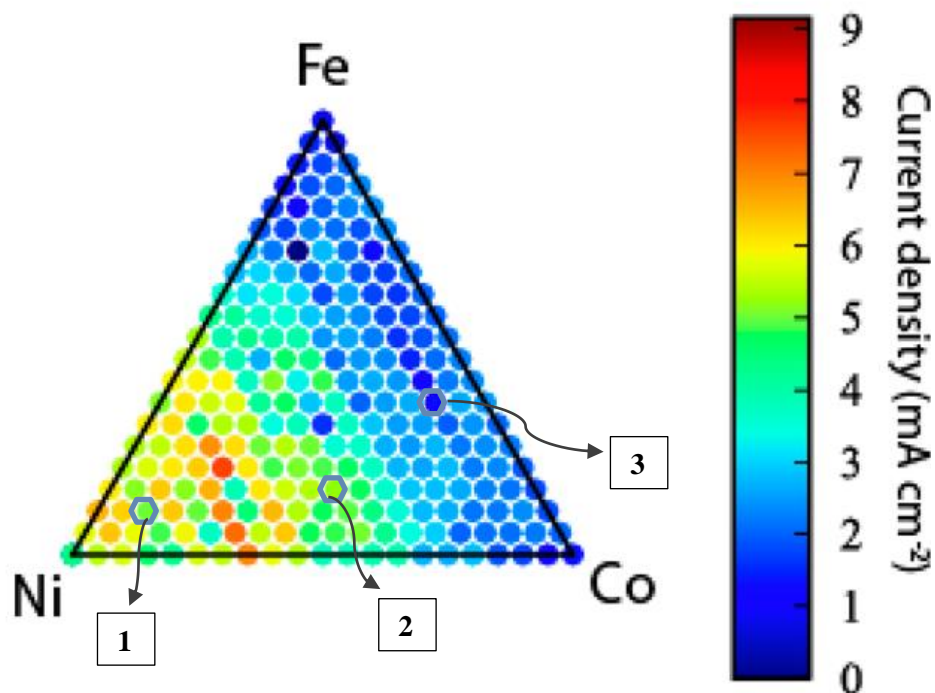


Figure 3.14. (Ni-Fe-Co) O_x compositional scan (@750 mV vs Ag/AgCl)

(Reprinted with permission from ACS Comb. Sci. 2014, 16, 2, 47–52.

Copyright © 2014, American Chemical Society.)

It has been concluded that the differences may be due to dissimilar clogging percentage of the nozzles of each catalyst. Inkjet printhead cleaning procedure was employed before continuing with another experiment.

Clogging is one of the drawbacks in printing. Formulated inks must have appropriate dispersed particle size, viscosity, surface tension and volatility to prevent this phenomenon. Since the inkjet printheads are not standard the only method to improve an ink solution is trial and error.

3.1.2.3.1.2. Results and Discussion

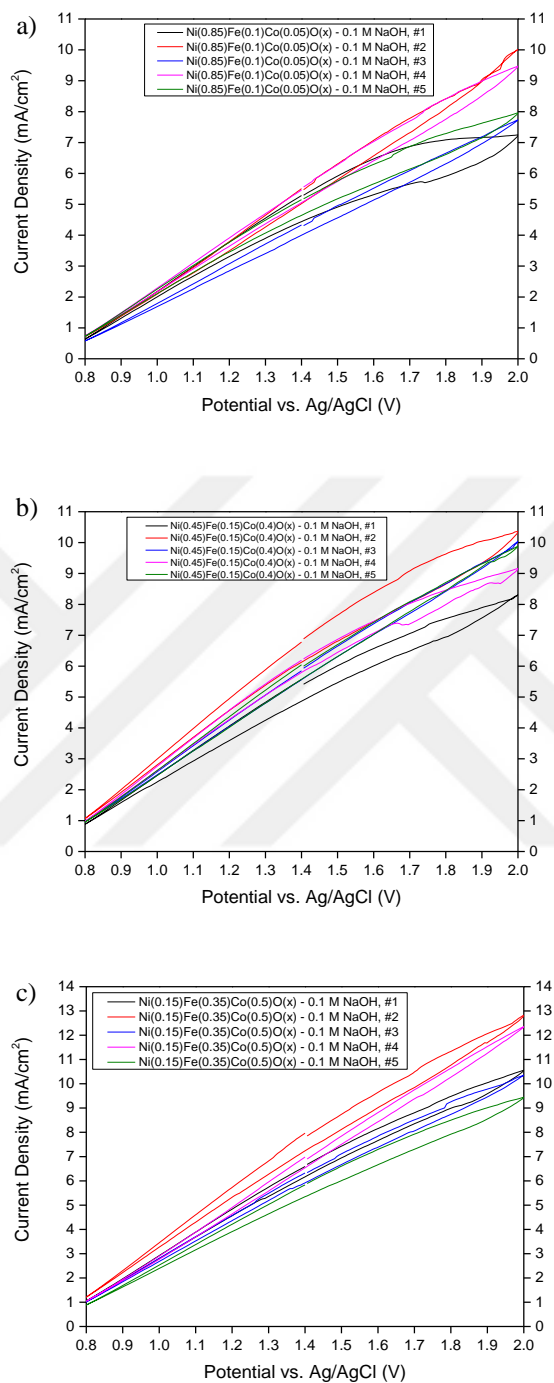


Figure 3.15. Cyclic voltammograms of printed a) Ni_{0.85}Fe_{0.1}Co_{0.05}O_x, b) Ni_{0.45}Fe_{0.15}Co_{0.4}O_x, c) Ni_{0.15}Fe_{0.35}Co_{0.5}O_x catalysts in 0.1 M NaOH electrolyte with a scan rate of 50mV/s.

Table 3.5. Overpotential measurements for printed $\text{Ni}_{0.85}\text{Fe}_{0.1}\text{Co}_{0.05}\text{O}_x$,
 $\text{Ni}_{0.45}\text{Fe}_{0.15}\text{Co}_{0.4}\text{O}_x$ and $\text{Ni}_{0.15}\text{Fe}_{0.35}\text{Co}_{0.5}\text{O}_x$ catalyst samples

Combination #	Current Density	Current Density in the
	<u>Measured</u>	<u>Article</u>
	@ 1660 mV (mA/cm ²)	@ 750 mV (mA/cm ²)
Ni_{0.85}Fe_{0.1}Co_{0.05}O_x - #1	6.74	6.5
Ni_{0.85}Fe_{0.1}Co_{0.05}O_x - #2	7.52	
Ni_{0.85}Fe_{0.1}Co_{0.05}O_x - #3	5.88	
Ni_{0.85}Fe_{0.1}Co_{0.05}O_x - #4	7.44	
Ni_{0.85}Fe_{0.1}Co_{0.05}O_x - #5	6.65	
Average	6.85	
Standard Deviation	0.67	
Standard Deviation %	9.77	
<hr/>		
Ni_{0.45}Fe_{0.15}Co_{0.4}O_x - #1	6.86	5.5
Ni_{0.45}Fe_{0.15}Co_{0.4}O_x - #2	8.77	
Ni_{0.45}Fe_{0.15}Co_{0.4}O_x - #3	7.78	
Ni_{0.45}Fe_{0.15}Co_{0.4}O_x - #4	7.84	
Ni_{0.45}Fe_{0.15}Co_{0.4}O_x - #5	7.83	
Average	7.82	
Standard Deviation	0.68	
Standard Deviation %	8.64	
<hr/>		
Ni_{0.15}Fe_{0.35}Co_{0.5}O_x - #1	8.56	3
Ni_{0.15}Fe_{0.35}Co_{0.5}O_x - #2	10.15	
Ni_{0.15}Fe_{0.35}Co_{0.5}O_x - #3	8.25	
Ni_{0.15}Fe_{0.35}Co_{0.5}O_x - #4	9.39	
Ni_{0.15}Fe_{0.35}Co_{0.5}O_x - #5	7.68	
Average	8.81	
Standard Deviation	0.97	
Standard Deviation %	11.05	

3.1.2.3.2. Compositional Scan of Nickel, Cobalt and Copper Oxides

3.1.2.3.2.1. Experimental Procedure

NiO, Co₃O₄ and CuO catalyst combinations with compositions changing at 33.3% intervals were printed on F:SnO₂/glass substrate at the center of the tray with SIZ+ Inkjet Material Printer. Also to test the position homogeneity, catalysts #6 - #10 had the same composition of NiCoCuO_x, printed in different regions shown below:

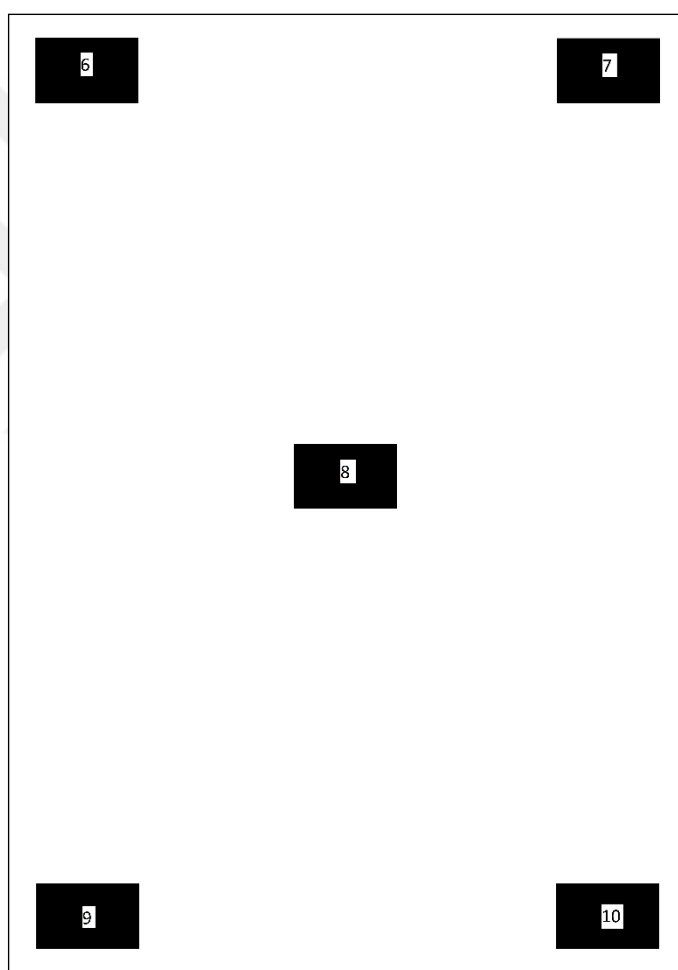


Figure 3.16. Tray positions for printed NiCoCuO_x catalysts #6 - #10

Printed catalysts were calcined at 40°C for 18 h, at 70°C for 24 h, at 350°C for 10 h, respectively.

Electrochemical measurements were taken using CV in a three-electrode system with an Autolab PGSTAT204 potentiostat. Ag/AgCl was used as the reference electrode and Pt mesh was used as the counter electrode while catalysts printed on a F:SnO₂/glass were employed as the working electrodes. As the electrolyte, 1 M KOH was used for all of the catalysts with a scan rate of 100 mV/s. Current densities were measured against the voltage vs RHE, which is calculated considering the theoretical pH of the electrolyte (pH=14 for 1 M KOH) according to the formula:

$$E_{RHE} = E_{measured} + E_{Ag/AgCl} + 0.059 \cdot pH \quad (6)$$

($E_{Ag/AgCl} = 0.205$ V for electrode stored in 3.5 M KCl)

3.1.2.3.2.2. Results and Discussion

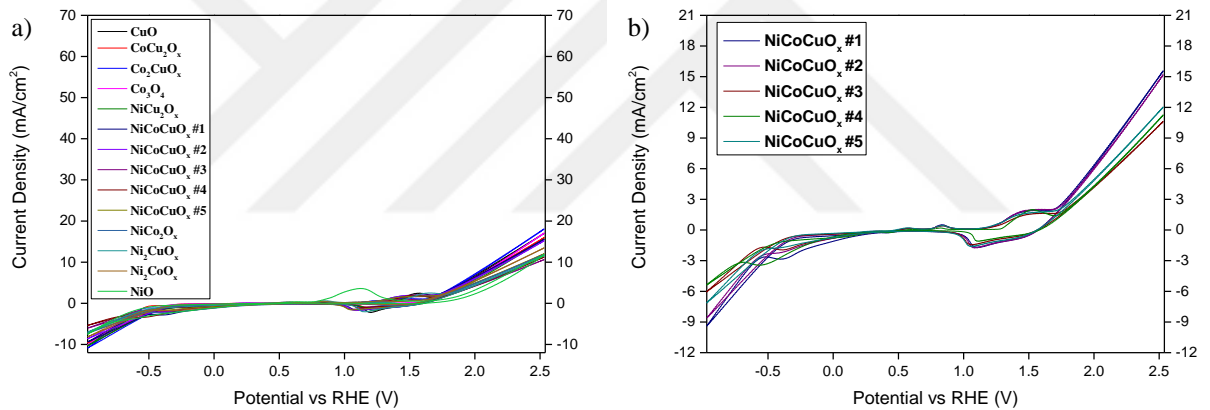


Figure 3.17. Cyclic voltammograms of a) printed Ni_xCo_yCu_zO_n catalysts in 0.1 M KOH electrolyte with a scan rate of 100mV/s, b) NiCoCuO_x catalysts located in different parts of the tray

Water oxidation overpotentials (η) given in the table below were calculated by the following formula:

$$\eta = E_{measured} - 1.23 \quad (7)$$

Table 3.6. Water oxidation overpotential measurements for printed Ni_xCo_yCu_zO_n catalyst samples @10 mA/cm²

Catalyst #	Overpotential (mV) (@10 mA/cm ²)
#1 - CuO	940
#2 - CoCu ₂ O _x	979
#3 - Co ₂ CuO _x	913
#4 - Co ₃ O ₄	967
#5 - NiCu ₂ O _x	1006
#6 - NiCoCuO _x	987
#7 - NiCoCuO _x	1006
#8 - NiCoCuO _x	1250
#9 - NiCoCuO _x	1211
#10 - NiCoCuO _x	1153
Average (#6 - #10)	1121.4
SD (#6 - #10)	119.32
SD % (#6 - #10)	10.64
#11 - NiCo ₂ O _x	1162
#12 - Ni ₂ CuO _x	1187
#13 - Ni ₂ CoO _x	1074
#14 - NiO	1189

Overpotential values of different compositions showed similar values which would lead to further experiments depending on the relation between the overpotential and the optimum layer count. Measurements #6-#10 also revealed that overpotential

values depend on the position of the printed catalyst on the tray. There is a variation about 11% in measured potentials.

Besides different rate of blockage of the nozzles degradation during the electrochemical experiment may play a role in similar overpotential values. Measured overpotential values are parallel to the overpotentials of F:SnO₂/glass in Section 3.3 which is a clue for the detachment of the catalysts.

To overcome this complexity further single metal oxide experiments relating to catalyst loading and homogeneity must be performed.

3.2. Effect of Film Homogeneity

3.2.1. Experimental Procedure

Homogeneity in film formation and preventing the coffee-ring effect plays an important role in electronic conductivity of the film. This feature is obtained by either modifying the evaporation of the mixed solvent or enhancing the hydrophobicity of substrate.

In the article Lim et al. examined the morphology of inkjet-printed 6,13-bis((triisopropylsilyl)ethynyl) pentacene (TIPS_PEN) on 1,1,1,3,3,3-hexamethyldisilazane (HMDS) treated SiO₂ (Lim et al. 2008).

By adding an auxiliary solvent with a higher boiling point they enhanced the homogeneity. Addition of a solvent with a higher boiling point and a lower surface tension resulted in ordered crystalline structures. Surface tension gradient between the main and auxiliary solvent caused the marangoni flow which occurs through the reverse direction of the convection flow.

In a different article Oh et al. Investigated the uniformity of Al₂O₃ film on Pt coated Si wafer of [100] orientation. Similarly they used water as the main solvent and DMF as the drying agent (Oh et al. 2011).

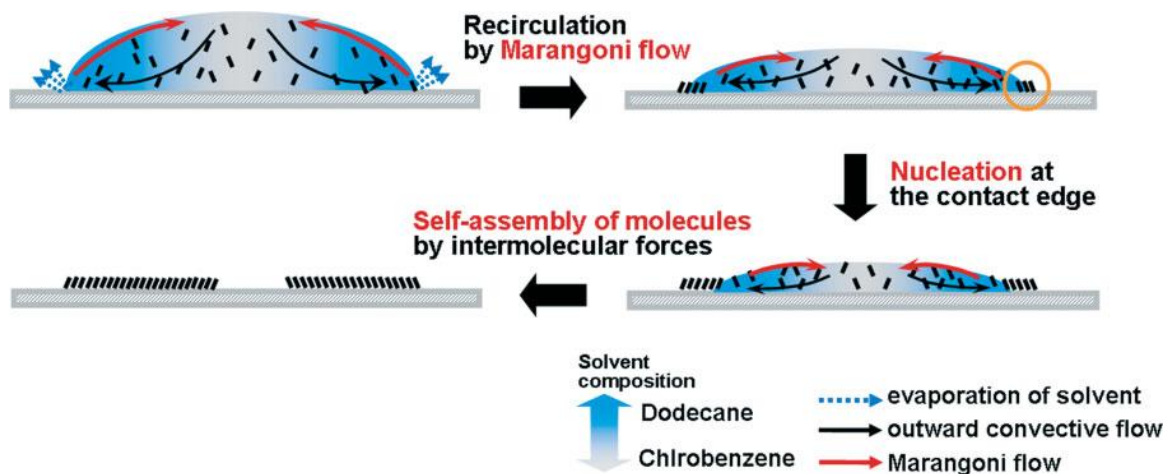


Figure 3.18. Forces governing evaporation induced film formation from a droplet.

(Reprinted from *Advanced Functional Materials*, Volume 18, Issue 2, J. A. Lim, W. H. Lee, H. S. Lee, J. H. Lee, Y. D. Park, K. Cho, Self-Organization of Ink-jet-Printed Triisopropylsilylethynyl Pentacene via Evaporation-Induced Flows in a Drying Droplet, Pages 229-234, Copyright © 2008 WILEY-VCH Verlag GmbH & Co. KGaA, Weinheim.)

In another study on the subject Kim et al. applied gradual heating on inkjet printed Ag-nanoparticle inks on polyimide substrate to overcome the coffee-ring effect by limiting the convection flow (Kim, Nogi, and Suganuma 2012). The observations were as follows: As the printed lines grow wider resistivity decreases as a function of homogeneity. On the contrary narrow lines showed higher resistances. They applied heat on these narrow lines in the 20 °C to 200 °C temperature range with a gradient of 3 °C min⁻¹ and saw that the resistivity decreased and reached the value of the wider lines (Kim, Nogi, and Suganuma 2012).

Besides the modification of ink solution and environmental conditions such as temperature gradient and relative humidity, wetting behaviour of the substrate can be tuned. Non-wetting surfaces are more resistant to drop spreading thus improving the hydrophobicity of the substrate plays a relatively important role (Zhan et al. 2017).

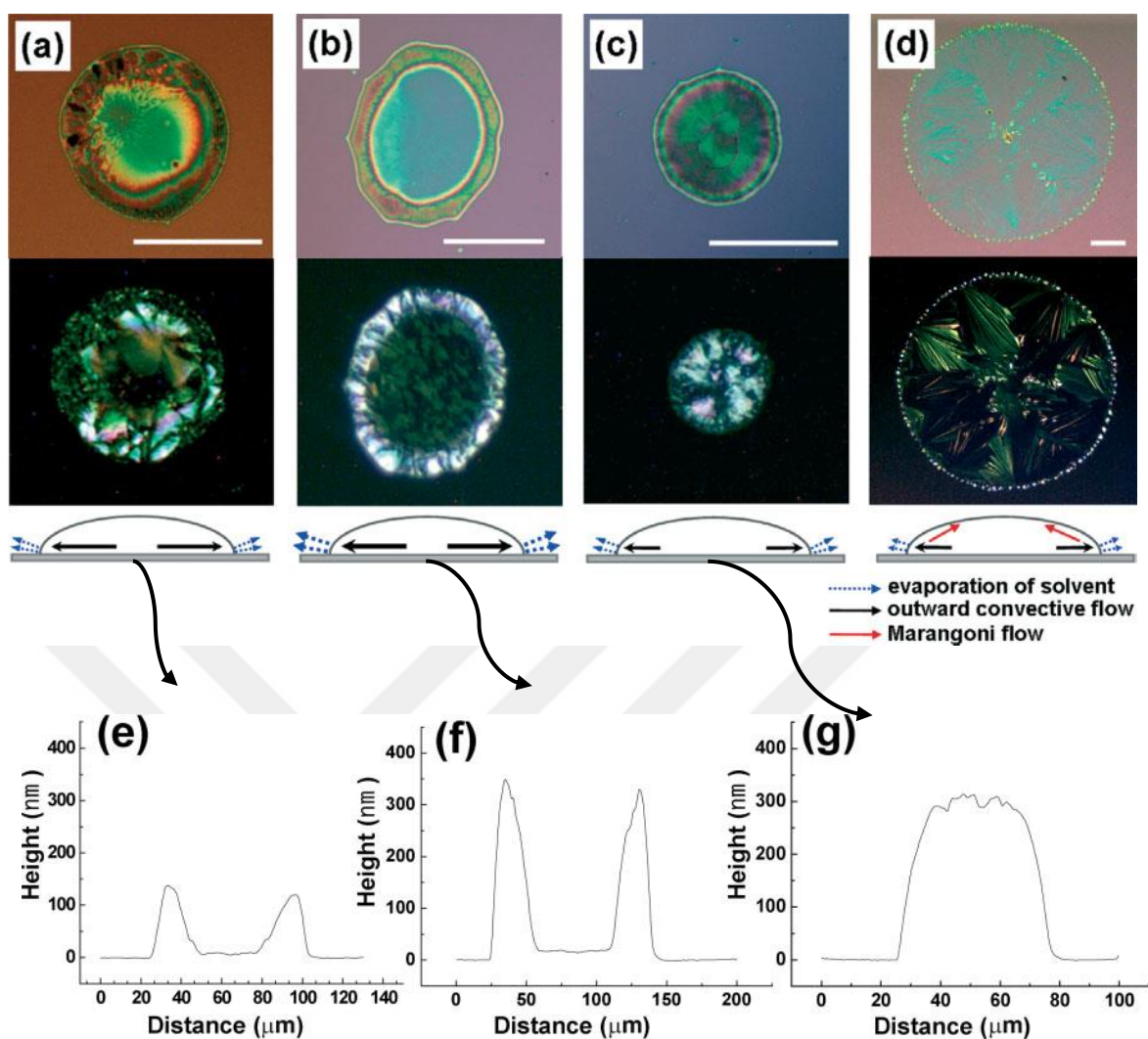


Figure 3.19. Optical microscope (OM) and polarized images of ink-jet-printed TIPS_PEN droplets with various solvent compositions: a) chlorobenzene and mixed-solvents containing chlorobenzene and 25 vol % b) hexane, c) o-dichlorobenzene, and d) dodecane. The height profiles of the TIPS_PEN single dots printed from e) chlorobenzene and the solvent mixture containing chlorobenzene and 25 vol %, f) hexane, and g) dichlorobenzene are shown at the bottom (scale bar = 50 μm). (Reprinted from *Advanced Functional Materials*, Volume 18, Issue 2, J. A. Lim, W. H. Lee, H. S. Lee, J. H. Lee, Y. D. Park, K. Cho, Self-Organization of Ink-jet-Printed Triisopropylsilylethynyl Pentacene via Evaporation-Induced Flows in a Drying Droplet, Pages 229-234, Copyright © 2008 WILEY-VCH Verlag GmbH & Co. KGaA, Weinheim.)

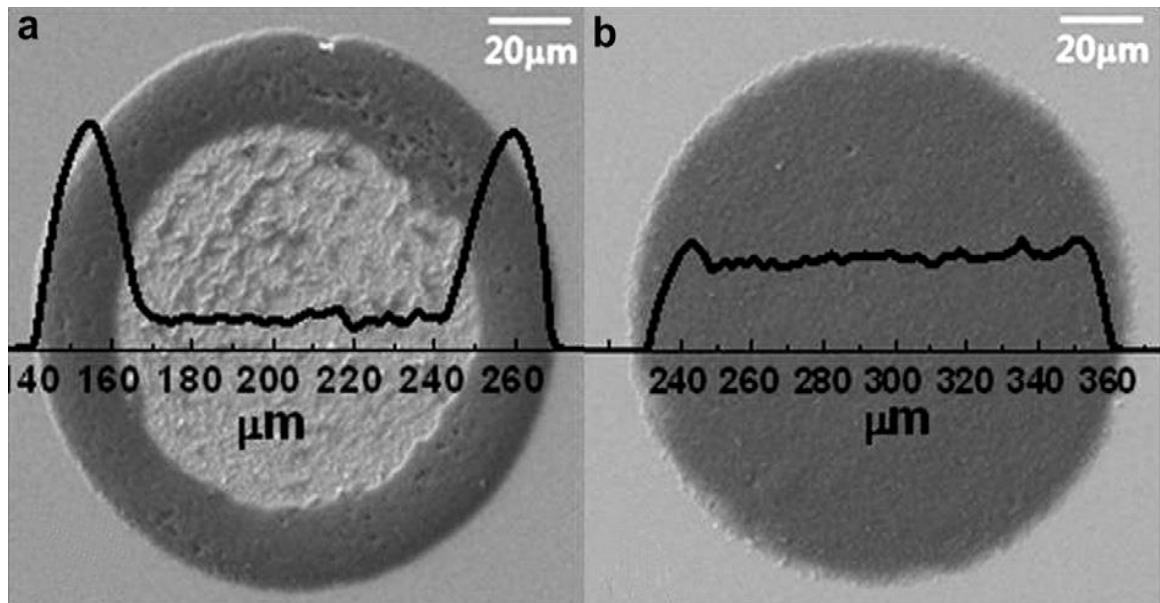


Figure 3.20. SEM images and surface profiles of Al_2O_3 ink droplets: (a) water single-solvent ink and (b) DMF + water co-solvent ink. (Reprinted from *Current Applied Physics*, Volume 11, Issue 3, Supplement, Yeonjun Oh, Jihoon Kim, Young Joon Yoon, Hyotae Kim, Ho Gyu Yoon, Sung-Nam Lee, Jonghee Kim, Inkjet printing of Al_2O_3 dots, lines, and films: From uniform dots to uniform films, Pages S359-S363, Copyright © 2011, with permission from Elsevier.)

Regarding the literature, in our inks based on ethanol, glycerol and acetic acid we can use the following co-solvents. Considering the higher boiling point and lowest surface tension dodecane seems to be the most appropriate solvent.

Based on the article used for ink preparation (Liu et al. 2012), using dodecane in the quaternary solvent mixture satisfies the surface tension (20-55 dyn/cm) and viscosity (5-30 mPa.s) range criterion. Therefore an experiment was performed with Ni ink including dodecane in 0, 10, 25, 50%, respectively.

On the other hand for modifying the substrate besides the C_4H_8 plasma treatment, one of the widely used method for hydrophobicity is silanization of the substrate.

Silanization was done using trimethoxy(octadecyl)silane after making F:SnO₂/glass surfaces hydrophilic by treatment with piranha solution.

Table 3.7. Appropriate co-solvents and related properties

	Boiling Point (°C)	Surface Tension (mN/m)	Viscosity @RT (cP)
DMF	153	37.1	0.92
Dimethyl acetamide	165	34	2.14
Ethylene-glycol	197.6	47.99	21
Diethylene-glycol	180-190	44.8	35.7
DMSO	189	43.53	2.24
Dodecane	216	25.3	1.36
Nitrobenzene	211	46.34	1.86
Phenol	182	40.5	3.44

Pretreatment with piranha solution was done following the procedure in the reference (Subramani 2009). 60 mL, 50% (v/v) H₂SO₄ solution was mixed with 20 mL, 30% (w/v) H₂O₂ solution. F:SnO₂/glass coated glass substrates were immersed in the solution for 10 min, then rinsed with DI water and dried in N₂ atmosphere.

Silanization was done following the procedure in the reference article (Gabriunaite, Valiūnienė, and Valincius 2018). For silanization 5 μL of trimethoxy(octadecyl)silane was dissolved in 10 mL heptane. Substrates were immersed in the solution at 60°C for 1 h, then rinsed with heptane to remove excess silane and dried in N₂ atmosphere.

Contact angle measurements were performed with the apparatus shown in the following picture. All contact angle measurements were done using ImageJ image processing program.

3.2.2. Results and Discussion

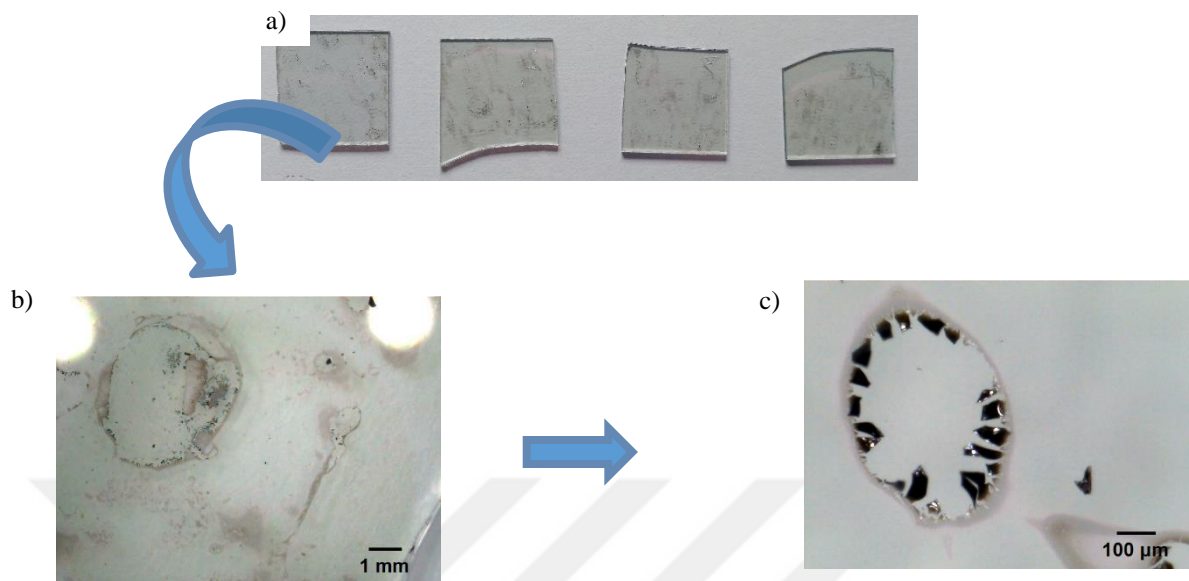


Figure 3.21. a) Sequentially printed NiO catalysts including 0, 10, 25, 50% dodecane, respectively. b), c) Optical microscopic image with different magnifications printed NiO catalyst including 10% dodecane.



Figure 3.22. Contact angle measurement apparatus

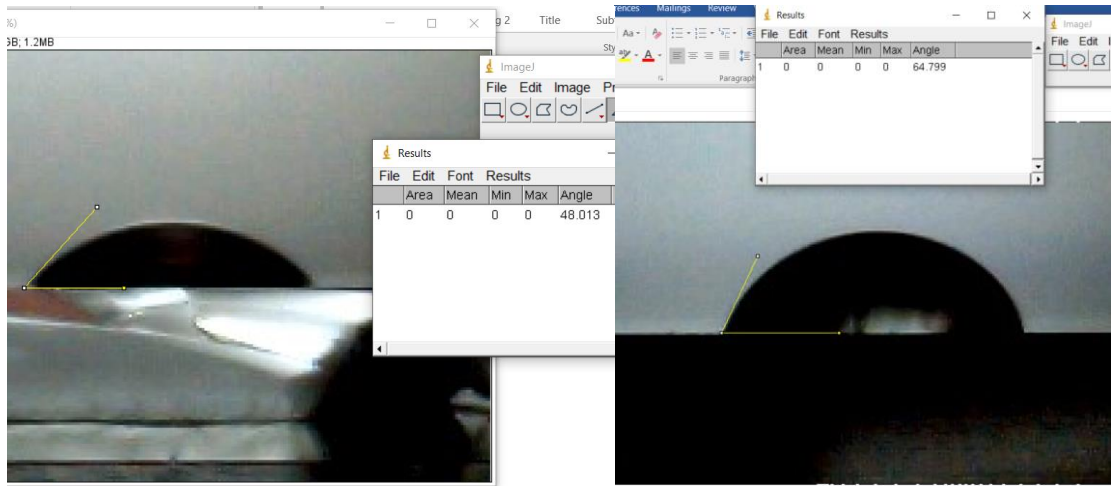


Figure 3.23. Contact angle measurement of pure water before and after silanization of F:SnO₂/glass, respectively.

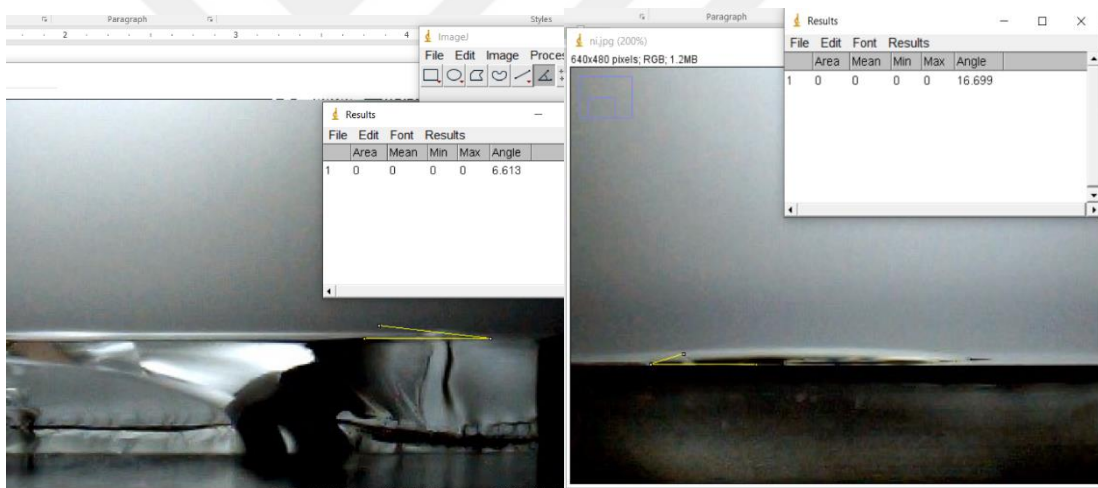


Figure 3.24. Contact angle measurement of Ni ink before and after silanization of F:SnO₂/glass, respectively.

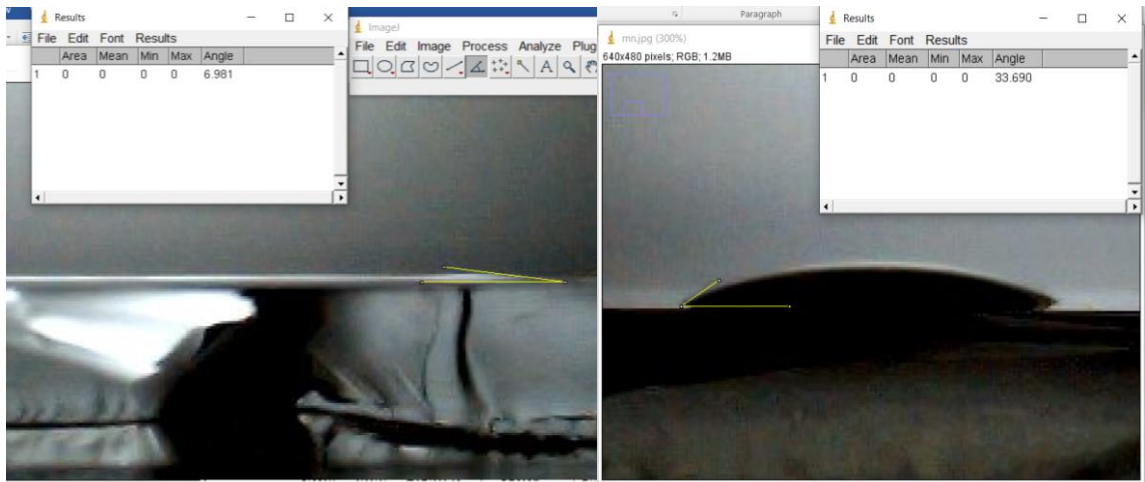


Figure 3.25. Contact angle measurement of Mn ink before and after silanization of F:SnO₂/glass, respectively.

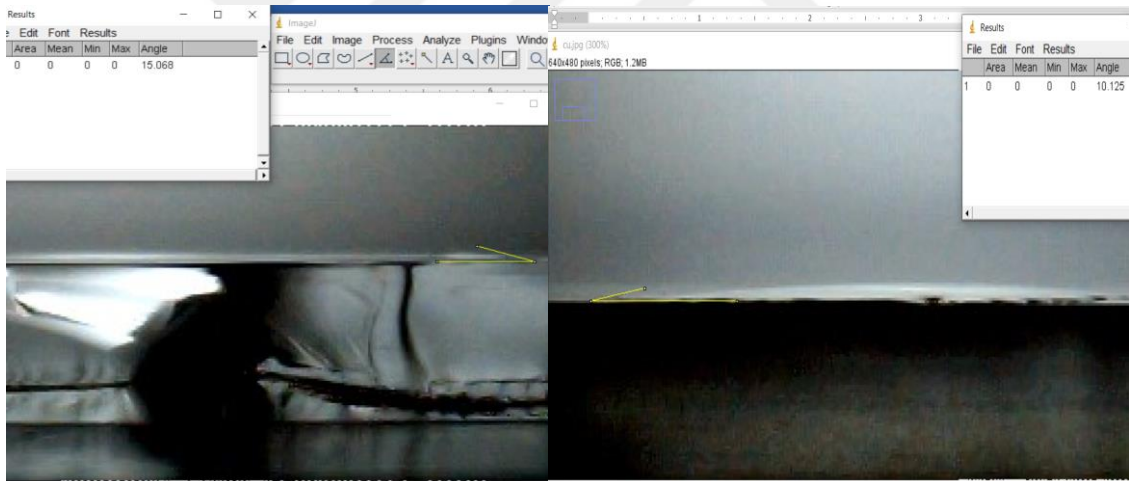


Figure 3.26. Contact angle measurement of Cu ink before and after silanization of F:SnO₂/glass, respectively.

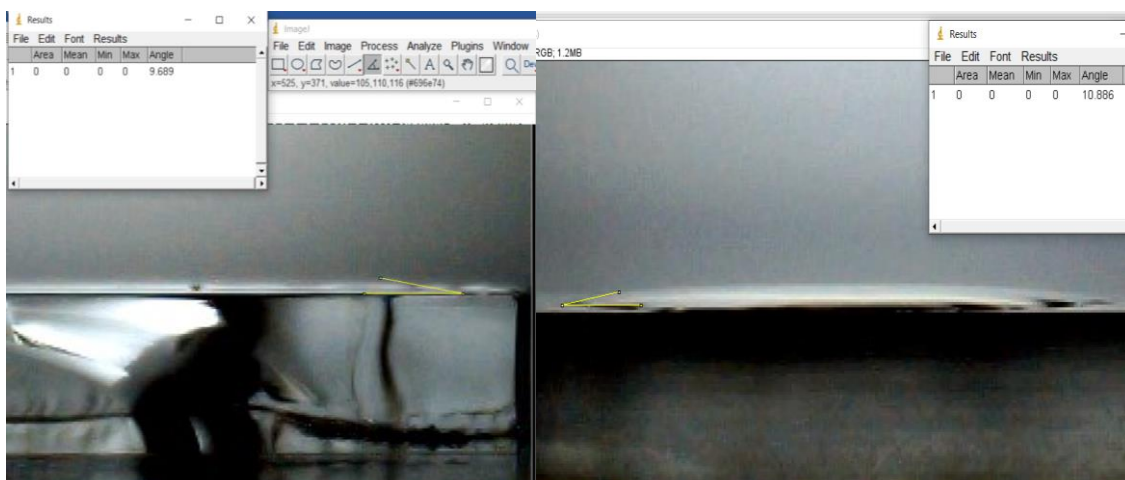


Figure 3.27. Contact angle measurement of Co ink before and after silanization of F:SnO₂/glass, respectively.

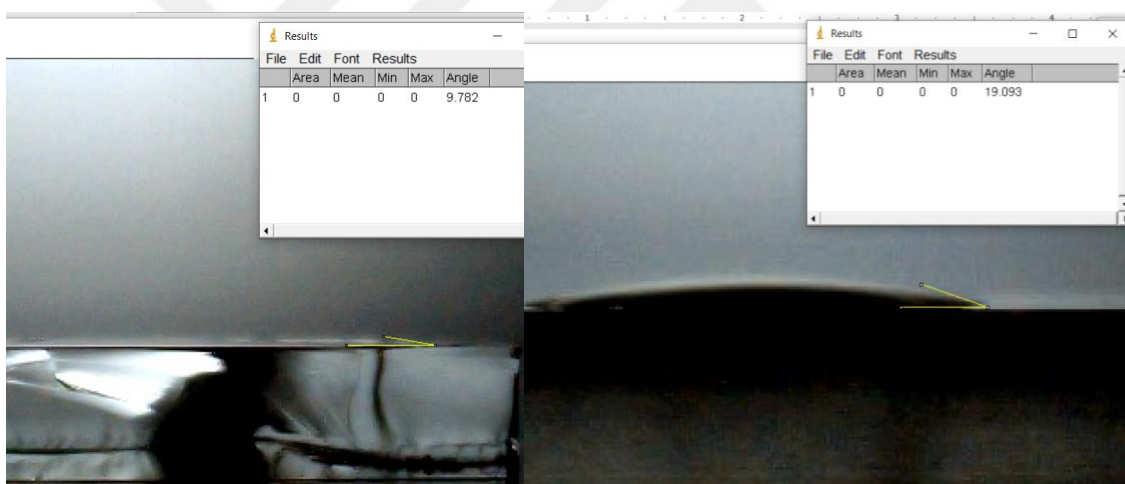


Figure 3.28. Contact angle measurement of Fe ink before and after silanization of F:SnO₂/glass, respectively.

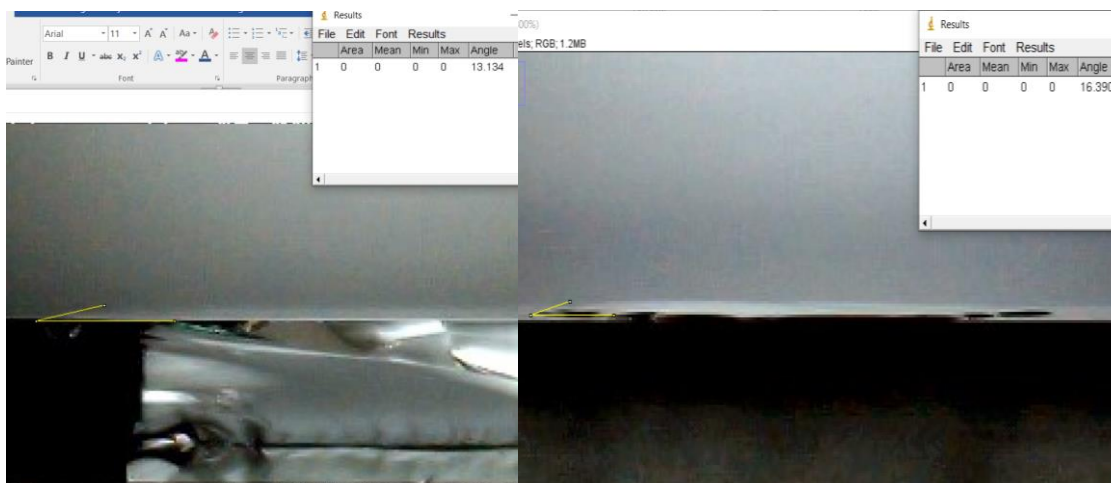


Figure 3.29. Contact angle measurement of Cr ink before and after silanization of F:SnO₂/glass, respectively.

Table 3.8. Contact angle measurements for pure water and printer inks

Drop on F:SnO ₂ /glass	Contact Angle	
	Before Silanization	After Silanization
Pure Water	48.01	64.8
Ni-ink	6.61	16.7
Mn-ink	6.98	33.69
Cu-ink	15.07	10.12
Co-ink	9.69	10.89
Fe-ink	9.78	19.09
Cr-ink	13.13	16.39

When dodecane was employed as co-solvent to induce Marangoni flow it was reported that the difference between the polarities of dodecane and ethanol prevented the homogeneity of the thin film formed. Microscopic images confirmed the increasing coffee-stain effect.

However an appropriate co-solvent with similar polarity, high boiling point and low surface tension may be investigated and employed for further studies. Ethanol, having a low surface tension limits the number of candidates. Therefore substitution of ethanol with another solvent with a higher surface tension would permit the utilization of many co-solvents.

It was clearly stated that silanization process was successful in enhancing the hydrophobicity of the substrate. To further study the effect of hydrophobicity of the substrate on morphologic and related electronic behavior of the catalyst thin film different proportions of a variety of silanizing agents having long alkyl chains could be employed. Also silanizing time and temperature may be increased for more effective hydrophobicity.

3.3. Comparison with Drop Casting Deposition Technique

3.3.1. Experimental Procedure

100 μ L(13 μ mol) NiO, Mn₃O₄ and Cr₂O₃ catalysts were deposited by drop method. To test precision, 5 samples were deposited for each catalyst, calcined at 40°C for 18 h, at 70°C for 24 h, at 350°C for 10 h, respectively.

Electrochemical measurements were taken using CV in a three-electrode system with an Autolab PGSTAT204 potentiostat. Ag/AgCl was used as the reference electrode and Pt mesh was used as the counter electrode while catalysts printed on a F:SnO₂/glass were employed as the working electrodes. As the electrolyte, 1 M KOH was used for all of the catalysts with a scan rate of 100 mV/s. Current densities were measured against the voltage vs RHE, which is calculated considering the pH of the electrolyte (pH=14 for 1 M KOH) according to the formula:

$$E_{\text{RHE}} = E_{\text{measured}} + E_{\text{Ag/AgCl}} + 0.059 \cdot \text{pH} \quad (6)$$

($E_{\text{Ag/AgCl}} = 0.205$ V for electrode stored in 3.5 M KCl)

Chronoamperometry measurements were taken after CV analysis of the best performed sample of each catalyst.

3.3.2. Results and Discussion

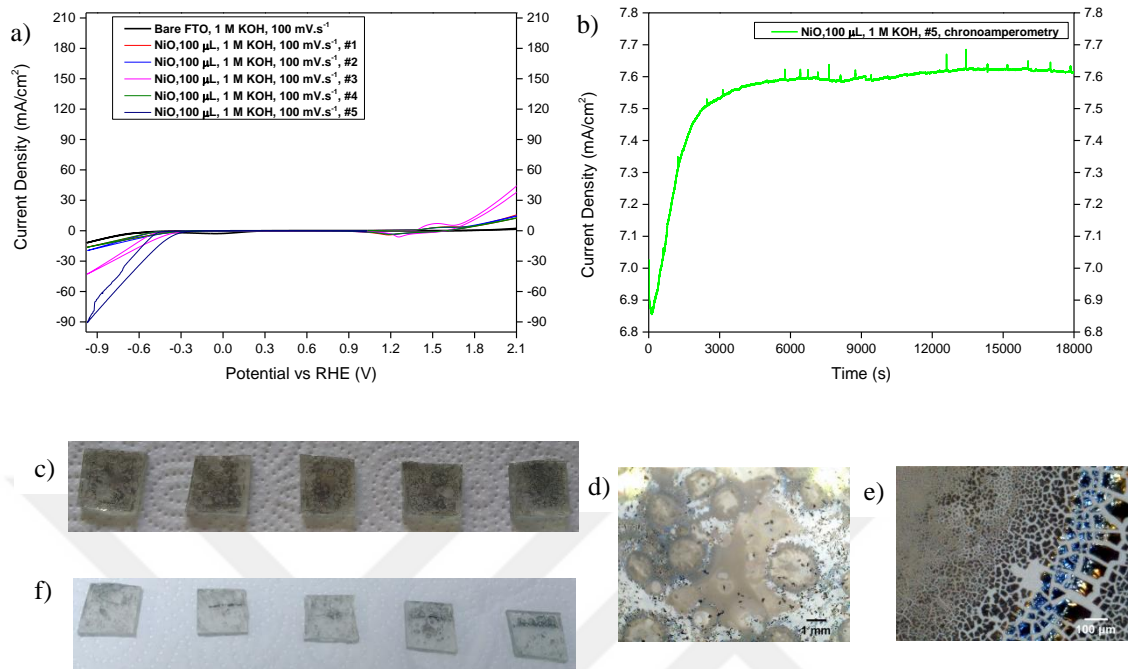


Figure 3.30. a) Precision of cyclic voltammograms for printed NiO catalyst in 1 M KOH electrolyte with a scan rate of 100mV/s b) Chronoamperometry of printed NiO catalyst in 1 M KOH electrolyte c) Sequentially printed NiO catalysts before cyclic voltammetry measurement d), e) Optical microscopic image with different magnifications printed NiO catalyst f) Sequentially printed NiO catalysts after cyclic voltammetry measurement

NiO shows the coffee-stain behavior more than the other catalysts as can be noticed in Figure 3.27. Also it includes an image of the catalysts after conducting the experiment was shown to address the degradation issue. Cyclic voltammogram of NiO shows the reversible oxidation peak of Ni^{2+} to Ni^{3+} at nearly 1.4 V.

Mn_3O_4 on the other hand shows a totally opposite behavior which is also known as mountain-top effect. Aggregation is obviously reducing the active surface area which results in higher overpotentials. In the first three sample 10 mA/cm^2 current range was out of the potential range of the experiment. The peak at nearly 0 V indicates the change in the oxidation state of Sn in the $\text{F:SnO}_2/\text{glass}$ substrate which stands as a clue of the

interface between bare F:SnO₂/glass and the electrolyte after degradation. It is obvious in the cyclic voltammograms of both Mn₃O₄ and Cr₂O₃.

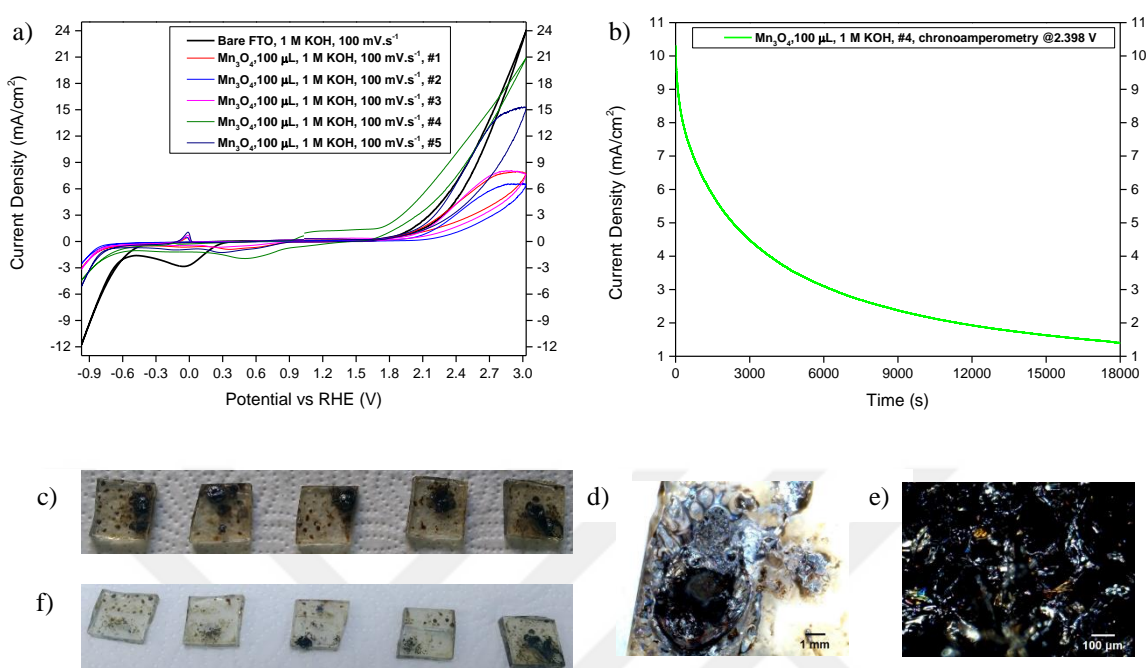


Figure 3.31. a) Precision of cyclic voltammograms for printed Mn₃O₄ catalyst in 1 M KOH electrolyte with a scan rate of 100mV/s b) Chronoamperometry of printed Mn₃O₄ catalyst in 1 M KOH electrolyte c) Sequentially printed Mn₃O₄ catalysts before cyclic voltammetry measurement d), e) Optical microscopic image with different magnifications printed Mn₃O₄ catalyst f) Sequentially printed Mn₃O₄ catalysts after cyclic voltammetry measurement

Cr₂O₃ catalysts were not totally adsorbed to F:SnO₂/glass surface during calcination while NiO and Mn₃O₄ catalysts were mostly adsorbed during calcination but detached substantially from the F:SnO₂/glass surfaces during CV measurements. This may explain why the standard deviation in Cr₂O₃ is the least among all catalysts and also the fluctuations in NiO measurements. The degradation can also be seen obviously in the Figure 3.29. Although these detachments also make it difficult to compare the measurements with inkjet-printed catalysts examining printed and drop casted sample overpotential measurements, inkjet printing noticeably lowered the deviation between samples which led us to think it is a reliable and more reproducible method for catalyst deposition.

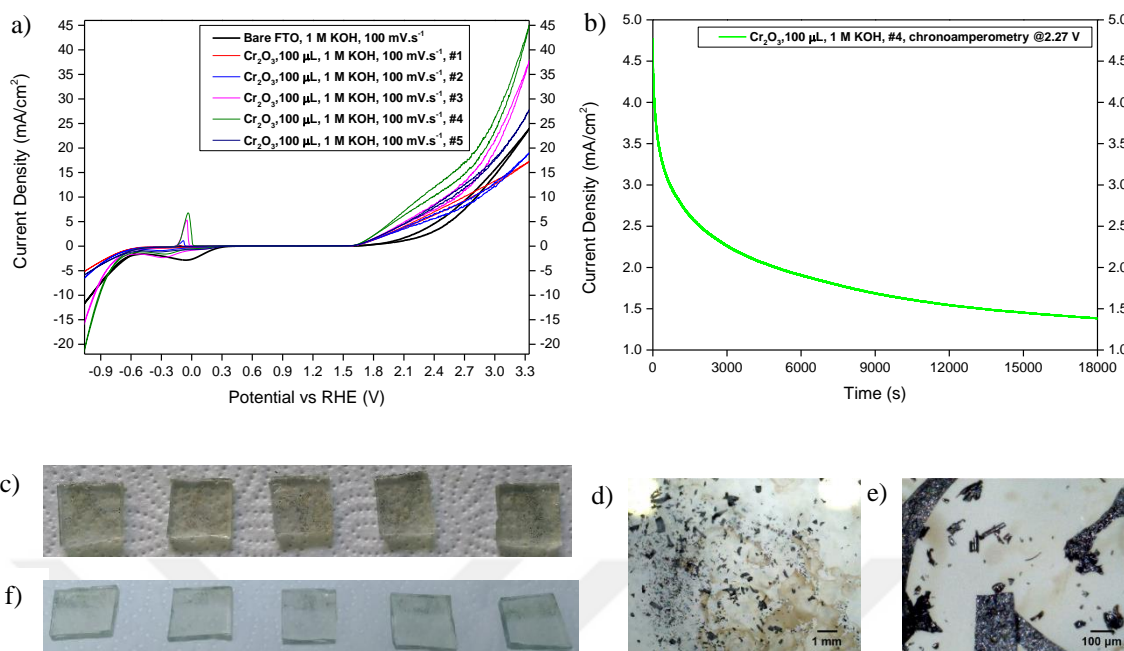


Figure 3.32. a) Precision of cyclic voltammograms for printed Cr_2O_3 catalyst in 1 M KOH electrolyte with a scan rate of 100mV/s b) Chronoamperometry of printed Cr_2O_3 catalyst in 1 M KOH electrolyte c) Sequentially printed Cr_2O_3 catalysts before cyclic voltammetry measurement d), e) Optical microscopic image with different magnifications printed Cr_2O_3 catalyst f) Sequentially printed Cr_2O_3 catalysts after cyclic voltammetry measurement

Besides, chronoamperometry results show that in the first 3000 seconds current density of NiO increased slightly while Mn_3O_4 and Cr_2O_3 performances decreased by half.

Overpotentials (η) given in the table below were calculated by the following formula:

$$\eta = E_{\text{measured}} - 1.23 \quad (7)$$

Table 3.9. Overpotential measurements for bare F:SnO₂/glass and drop casted NiO, Mn₃O₄ and Cr₂O₃ catalyst samples

Catalyst #	Overpotential Measured, (mV)		Overpotential in Article, (mV)
	(@10 mA/cm ²)	Onset (0.1 mA/cm ²)	(Onset)
Bare F:SnO ₂ /glass - #1	997	365	500
Bare F:SnO ₂ /glass - #2	1176	365	(Benck 2014)
Bare F:SnO ₂ /glass - #3	962	348	
Bare F:SnO ₂ /glass - #4	1118	377	
Average	1063.25	363.75	
Standard Deviation	100.58	11.93	
Standard Deviation %	9.46	3.28	
	(@10 mA/cm ²)		(@10 mA/cm ²)
NiO - #1	729		420 (McCrorry 2013)
NiO - #2	724		
NiO - #3	524		
NiO - #4	773		
NiO - #5	509		
Average	651.8		
Standard Deviation	125.09		
Standard Deviation %	19.19		
	(@10 mA/cm ²)		(@10
Mn ₃ O ₄ - #1	-		570
Mn ₃ O ₄ - #2	-		(Ramírez 2014)
Mn ₃ O ₄ - #3	-		
Mn ₃ O ₄ - #4	1168		
Mn ₃ O ₄ - #5	1322		
Average	1245		
Standard Deviation	108.89		
Standard Deviation %	8.75		
	(@10 mA/cm ²)		
Cr ₂ O ₃ - #1	1459		-

(cont. on next page)

Table 3.9 (cont.)

Cr ₂ O ₃ - #2	1559
Cr ₂ O ₃ - #3	1285
Cr ₂ O ₃ - #4	1040
Cr ₂ O ₃ - #5	1293
Average	1372.7
Standard Deviation	197.82
Standard Deviation %	14.41



CHAPTER 4

CONCLUSIONS AND OUTLOOKS

Concluding the experiments, the issues to be considered in the production of catalysts via inkjet printing and what can be done to overcome those are summarized below.

It was observed that the inks could cause corrosion in the channels inside the inkjet printhead due to their strong acidity. This observation is based on the presence of mixture of colors in the printed output, with each ink having different colors. The most corrosive ink was found to be iron ink. Therefore after each print, the retention time of the inks in the inkjet printhead was minimized by the ethanol washing procedure. For subsequent studies, it is suggested to decrease the corrosivity of the inks by increasing pH values.

In addition, taking into account the increase in viscosity to reduce the volatility of the inks, higher carbon alcohols may be used instead of ethanol in the ink formulation or it may be necessary to control ambient temperature and relative humidity.

Moreover, the distance between the tray and the inkjet printhead must be minimized in order to obtain the prints at the highest resolution.

Considering that the catalyst sample coated on the surface of the F:SnO₂/glass could detach while in contact with the electrolyte and in the presence of voltage, it may be more reliable to repeat the experiments more than once and obtain an average value. However, procedures can be developed to increase the adhesion of the deposited catalysts to the surface. Increasing the bond formed by the catalyst with the substrate surface will yield much more accurate results as the catalysts coated on the substrate can be spilled into the calcination furnace or even during transfers. Similarly, deposition can be made on different substrates and degradation behavior can be monitored.

The current density obtained from the electrochemical measurement should be normalized not only by the surface area but also by catalyst loading for benchmarking studies. However, it is important to calculate the roughness factor and determine the electrochemically active surface area of the catalyst in order to obtain the accurate result. It is of great importance to determine the internal resistance of the electrochemical

reaction system before the measurements and to determine how much of it can be compensated. Finally although the potentials with respect to the reference electrode can be converted into RHE values depending on the type and solution concentration, the use of materials with different surface area and mass for the counter electrode may lead to divergence from standardization.

While converting the potential value measured versus Ag/AgCl electrode into RHE, pH values used in Nernst equation are theoretical in some literature while experimental measurements are used in others. However, the overpotential values to be obtained as a result of experimental measurement of pH value will be slightly lower than for the case of the theoretical ones. For this reason, in the future studies, it may be more accurate to prepare electrolytes with the same concentration more than once and to take into consideration the standard deviation of pH measurement.

If the number of prints to be taken to reach the literature value for each catalyst can be determined by trial and error, the comparison of the multi-metal oxides can be performed in a more accurate manner. On the other hand, onset potentials can be used as descriptors since they are independent of catalyst loading. However, since onset current density is rarely expressed numerically in the literature, there remains an uncertainty about its definition.

Calcination temperature, duration and temperature increase rate can be optimized by further experiments for homogeneous coating of the catalyst film without forming aggregates or coffee stains. Using a co-solvent with an appropriate polarity, a marangoni flow can be induced to balance the convective flow. Finally, the amount of silanizing agent used to make the substrate hydrophobic can be optimized by increasing the treatment time or temperature.

If one is to consider the limitation of catalyst loading through degradation, inkjet-printing would definitely be the choice to alter loading in picoliter scale.

Since the only metal oxide catalyst studied which shows the photoelectrocatalytic behavior is Fe_2O_3 for the OER reaction, the combination of iron with other inks should be emphasized following the creation of a procedure on multi-metal oxide syntheses. Or multi-metal oxide electrocatalysts with low overpotentials can be integrated into the mono or dual absorber to form a monolithic artificial leaf.

REFERENCES

- Administration, U.S. Energy Information. (2019). International Energy Outlook 2019 with projections to 2050. Washington, DC 20585: U.S. Department of Energy.
- Agency, International Renewable Energy. (2019). Hydrogen: A Renewable Energy Perspective. Abu Dhabi: IRENA.
- Atkins, Peter, Paula, Julio D., and Keeler, James. (2018). *Atkins' Physical Chemistry*. Italy: Oxford University Press.
- Benck, J.D., Pinaud, B.A., Gorlin, Y. and Jaramillo, T.F. (2014). "Substrate Selection for Fundamental Studies of Electrocatalysts and Photoelectrodes: Inert Potential Windows in Acidic, Neutral, and Basic Electrolyte." *PLOS ONE* 9 (10):e107942.
- Cochran, Elizabeth A., Keenan N. Woods, Darren W. Johnson, Catherine J. Page, and Shannon W. Boettcher. (2019). "Unique chemistries of metal-nitrate precursors to form metal-oxide thin films from solution: materials for electronic and energy applications." *Journal of Materials Chemistry A* 7 (42):24124-24149. doi: 10.1039/C9TA07727H.
- Costa Bassetto, Victor, Jingjing Xiao, Emad Oveisi, Véronique Amstutz, Baohong Liu, Hubert H. Girault, and Andreas Lesch. (2018). "Rapid inkjet printing of high catalytic activity Co₃O₄/N-rGO layers for oxygen reduction reaction." *Applied Catalysis A: General* 563:9-17.
- Elezovic, N.R., Jovic, V.D., and Krstajic, N.V. (2005). "Kinetics of the hydrogen evolution reaction on Fe–Mo film deposited on mild steel support in alkaline solution." *Electrochimica Acta* 50:5594–5601.
- Fan, Chonglun, Piron, D. L. and Paradis, P. (1994a). "Hydrogen evolution on electrodeposited nickel-cobalt-molybdenum in alkaline water electrolysis." *Electrochimica Acta* 39:2715-2722.
- Fan, Chonglun, Piron, D. L., Sleb, Abderrahman and Paradis, P. (1994b). "Study of Electrodeposited Nickel–Molybdenum, Nickel–Tungsten, Cobalt–Molybdenum, and Cobalt–Tungsten as Hydrogen Electrodes in Alkaline Water Electrolysis." *J. Electrochem. Soc.* 141 (2):382-387.

- Fujishima, Akira and Honda, Kenichi. (1972). "Electrochemical Photolysis of Water at a Semiconductor Electrode." *Nature* 238:37-38.
- Gabriunaite, Inga, Aušra Valiūnienė, and Gintaras Valincius. (2018). "Formation and properties of phospholipid bilayers on fluorine doped tin oxide electrodes." *Electrochimica Acta* 283:1351-1358.
- Gahlawat, Soniya, Nusrat Rashid, and Pravin P. Ingole. (2018). "n-Type Cu₂O/ α -Fe₂O₃ Heterojunctions by Electrochemical Deposition: Tuning of Cu₂O Thickness for Maximum Photoelectrochemical Performance." *Zeitschrift für Physikalische Chemie* 232 (9-11):1551.
- Haber, Joel A., Yun Cai, Suho Jung, Chengxiang Xiang, Slobodan Mitrovic, Jian Jin, Alexis T. Bell, and John M. Gregoire. (2014). "Discovering Ce-rich oxygen evolution catalysts, from high throughput screening to water electrolysis." *Energy & Environmental Science* 7 (2):682-688.
- Heller, A., Aharon-Shalom, E., Bonner, W.A., and Miller, B. (1982). "Hydrogen-Evolving Semiconductor Photocathodes. Nature of the Junction and Function of the Platinum Group Metal Catalyst." *J. Am. Chem. Soc.* 104:6942-6948.
- Ho, J.C.K., and Piron, D.L. (1996). "Active surface area in oxide electrodes by overpotential deposited oxygen species for the oxygen evolution reaction." *Journal of Applied Electrochemistry* 26:515-521.
- IRENA. 2019. Global energy transformation: A roadmap to (2050) (2019 edition). Abu Dhabi: International Renewable Energy Agency.
- Jafarian, M., O. Azizi, F. Gobal, and M. G. Mahjani. (2007). "Kinetics and electrocatalytic behavior of nanocrystalline CoNiFe alloy in hydrogen evolution reaction." *International Journal of Hydrogen Energy* 32 (12):1686-1693.
- Jafarian, M., Azizi, O., Gobal, F., and Mahjani, M.G. (2007). "Kinetics and electrocatalytic behavior of nanocrystalline CoNiFe alloy in hydrogen evolution reaction." *International Journal of Hydrogen Energy* 32:1686–1693.
- Jayalakshmi, M., Kim, Woo-Young, Jung, Kwang-Deog, Joo, Oh-Shim. (2008). "Electrochemical Characterization of Ni-Mo-Fe Composite Film in Alkali Solution." *Int. J. Electrochem. Sci.* 3:908 - 917.
- Khaselev, Oscar, and Turner, John, A. (1998). "A Monolithic Photovoltaic-Photoelectrochemical Device for Hydrogen Production via Water Splitting." *Science* 280:425-427.

- Kim, Changjae, Masaya Nogi, and Katsuaki Sukanuma. (2012). "Electrical conductivity enhancement in inkjet-printed narrow lines through gradual heating." *Journal of Micromechanics and Microengineering* 22 (3):035016. doi: 10.1088/0960-1317/22/3/035016.
- Kuang, Minxuan, Libin Wang, and Yanlin Song. (2014). "Controllable Printing Droplets for High-Resolution Patterns." *Advanced Materials* 26 (40):6950-6958. doi: 10.1002/adma.201305416.
- Li, Xiaohong, Walsh, Frank C. and Pletcher, Derek (2011). "Nickel based electrocatalysts for oxygen evolution in high current density, alkaline water electrolyzers." *Phys. Chem. Chem. Phys.* 13:1162–1167.
- Lim, J. A., W. H. Lee, H. S. Lee, J. H. Lee, Y. D. Park, and K. Cho. (2008). "Self-Organization of Ink-jet-Printed Triisopropylsilylethynyl Pentacene via Evaporation-Induced Flows in a Drying Droplet." *Advanced Functional Materials* 18 (2):229-234.
- Liu, Xiang, Shengsheng Cui, Manman Qian, Zijun Sun, and Pingwu Du. (2016). "In situ generated highly active copper oxide catalysts for the oxygen evolution reaction at low overpotential in alkaline solutions." *Chemical Communications* 52 (32):5546-5549.
- Liu, Xiaonao, Yi Shen, Ruoting Yang, Shihui Zou, Xiulei Ji, Lei Shi, Yichi Zhang, Deyu Liu, Liping Xiao, Xiaoming Zheng, Song Li, Jie Fan, and Galen D. Stucky. (2012). "Inkjet Printing Assisted Synthesis of Multicomponent Mesoporous Metal Oxides for Ultrafast Catalyst Exploration." *Nano Letters* 12 (11):5733-5739.
- Martin, G. D., S. D. Hoath, and I. M. Hutchings. (2008). "Inkjet printing - the physics of manipulating liquid jets and drops." *Journal of Physics: Conference Series* 105:012001.
- McCrory, C.C.L., Jung, S., Ferrer, I.M., Chatman, S.M., Peters, J.C., and Jaramillo, T.F. (2015). "Benchmarking Hydrogen Evolving Reaction and Oxygen Evolving Reaction Electrocatalysts for Solar Water Splitting Devices." *J. Am. Chem. Soc.* 137:4347–4357.
- McCrory, C.C.L., Jung, S., Peters, J.C., and Jaramillo, T.F. (2013). "Benchmarking Heterogeneous Electrocatalysts for the Oxygen Evolution Reaction." *J. Am. Chem. Soc.* 135:16977–16987.
- McCrory, Charles C. L., Suho Jung, Ivonne M. Ferrer, Shawn M. Chatman, Jonas C. Peters, and Thomas F. Jaramillo. (2015). "Benchmarking Hydrogen Evolving Reaction and Oxygen Evolving Reaction Electrocatalysts for Solar Water Splitting Devices." *Journal of the American Chemical Society* 137 (13):4347-4357.

- McCrory, Charles C. L., Suho Jung, Jonas C. Peters, and Thomas F. Jaramillo. (2013). "Benchmarking Heterogeneous Electrocatalysts for the Oxygen Evolution Reaction." *Journal of the American Chemical Society* 135 (45):16977-16987.
- Merki, Daniel, Stéphane Fierro, Heron Vrubel, and Xile Hu. (2011). "Amorphous molybdenum sulfide films as catalysts for electrochemical hydrogen production in water." *Chemical Science* 2 (7):1262-1267.
- Merrill, Matthew D., and Ralph C. Dougherty. (2008). "Metal Oxide Catalysts for the Evolution of O₂ from H₂O." *The Journal of Physical Chemistry C* 112 (10):3655-3666.
- Montoya, Joseph H., Linsey C. Seitz, Pongkarn Chakthranont, Aleksandra Vojvodic, Thomas F. Jaramillo, and Jens K. Nørskov. (2017). "Materials for solar fuels and chemicals." *Nature Materials* 16 (1):70-81.
- Niu, Siqi, Siwei Li, Yunchen Du, Xijiang Han, and Ping Xu. (2020). "How to Reliably Report the Overpotential of an Electrocatalyst." *ACS Energy Letters* 5 (4):1083-1087.
- Oh, Yeonjun, Jihoon Kim, Young Joon Yoon, Hyotae Kim, Ho Gyu Yoon, Sung-Nam Lee, and Jonghee Kim. (2011). "Inkjet printing of Al₂O₃ dots, lines, and films: From uniform dots to uniform films." *Current Applied Physics* 11 (3, Supplement):S359-S363.
- Ohashi, K., McCann, J., Bockris, J., O'M. (1977). "Stable photoelectrochemical cells for the splitting of water." *Nature*:610-611.
- Qin, Fan, Zhenhuan Zhao, Md Kamrul Alam, Yizhou Ni, Francisco Robles-Hernandez, Luo Yu, Shuo Chen, Zhifeng Ren, Zhiming Wang, and Jiming Bao. (2018). "Trimetallic NiFeMo for Overall Electrochemical Water Splitting with a Low Cell Voltage." *ACS Energy Letters* 3 (3):546-554.
- Raj, I., Arul, and Vasu, K.I. (1992). "Transition metal-based cathodes for hydrogen evolution in alkaline solution: electrocatalysis on nickel-based ternary electrolytic codeposits." *Journal of Applied Electrochemistry* 22:471-477.
- Raj, I., Arul, and, Vasu, K.I. (1990). "Transition metal-based hydrogen electrodes in alkaline solution - electrocatalysis on nickel based binary alloy coatings." *Journal of Applied Electrochemistry* 20:32-38.
- Ramírez, A., Hillebrand, P., Stellmach, D., May, M.M., Bogdanoff, P., and Fiechter, S. 2014. "Evaluation of MnO_x, Mn₂O₃, and Mn₃O₄ Electrodeposited Films for the Oxygen Evolution Reaction of Water." *J. Phys. Chem. C* 118:14073-14081.

- Ramírez, Alejandra, Philipp Hillebrand, Diana Stellmach, Matthias M. May, Peter Bogdanoff, and Sebastian Fiechter. 2014. "Evaluation of MnO_x, Mn₂O₃, and Mn₃O₄ Electrodeposited Films for the Oxygen Evolution Reaction of Water." *The Journal of Physical Chemistry C* 118 (26):14073-14081.
- Ranaweera, C. K., C. Zhang, S. Bhoyate, P. K. Kahol, M. Ghimire, S. R. Mishra, Felio Perez, Bipin Kumar Gupta, and Ram K. Gupta. 2017. "Flower-shaped cobalt oxide nano-structures as an efficient, flexible and stable electrocatalyst for the oxygen evolution reaction." *Materials Chemistry Frontiers* 1 (8):1580-1584.
- Reddington, Erik, Anthony Sapienza, Bogdan Gurau, Rameshkrishnan Viswanathan, S. Sarangapani, Eugene S. Smotkin, and Thomas E. Mallouk. 1998. "Combinatorial Electrochemistry: A Highly Parallel, Optical Screening Method for Discovery of Better Electrocatalysts." *Science* 280 (5370):1735.
- Santos, M.B.F., Peres Da Silva, E., Andrade JR, R., and Dias, J.A.F. (1992). "NiSn and Porous NiZn Coatings for Water Electrolysis." *Electrochimica Acta* 37:29-32.
- Savadogo, O., and Lavoie, H. (1992). "Hydrogen Evolution Reaction in an Alkaline Medium on Cobalt Electrodeposited with Heteropolyacids." *Int. J. Hydrogen Energy* 17:473-477.
- Solmaz, Ramazan and Kardas, Gülfeza. (2009). "Electrochemical deposition and characterization of NiFe coatings as electrocatalytic materials for alkaline water electrolysis." *Electrochimica Acta* 54:3726–3734.
- Spurgeon, Joshua M., Jesus M. Velazquez, and Matthew T. McDowell. (2014). "Improving O₂ production of WO₃ photoanodes with IrO₂ in acidic aqueous electrolyte." *Physical Chemistry Chemical Physics* 16 (8):3623-3631.
- Subramani, K. (2009). "Fabrication of hydrogel micropatterns by soft photolithography." *Emerging Nanotechnologies for Manufacturing*:279 - 291.
- Sun, Youyi, Yongji Zhang, Qing Liang, Yu Zhang, Huijun Chi, Yi Shi, and Daining Fang. (2013). "Solvent inkjet printing process for the fabrication of polymer solar cells." *RSC Advances* 3 (30):11925-11934.
- Terrett, Nicholas K., Mark Gardner, David W. Gordon, Ryszard J. Kobylecki, and John Steele. (1995). "Combinatorial synthesis — the design of compound libraries and their application to drug discovery." *Tetrahedron* 51 (30):8135-8173.
- Tsuji, Etsushi, Akihito Imanishi, Ken-ichi Fukui, and Yoshihiro Nakato. (2011). "Electrocatalytic activity of amorphous RuO₂ electrode for oxygen evolution in an aqueous solution." *Electrochimica Acta* 56 (5):2009-2016.

- Van de Krol, Roel, Gratzel, Michael. (2012). *Photoelectro-chemical Hydrogen Production*. Edited by H.L. Tuller. Springer New York Dordrecht Heidelberg London: Springer Science+Business Media, LLC.
- Van de Krol, Roel, Parkinson, Bruce, A. (2017). "Perspectives on the photoelectrochemical storage of solar energy." *MRS Energy & Sustainability* 4:1-11.
- Walton, D.J., Burke, L.D., and Murphy, M.M. (1996). "Sonoelectrochemistry: Chlorine, Hydrogen and Oxygen Evolution at Platinised Platinum." *Electrochimica Acta* 41:2747-2751.
- Xiang, Chengxiang, Santosh K. Suram, Joel A. Haber, Dan W. Guevarra, Ed Soedarmadji, Jian Jin, and John M. Gregoire. (2014). "High-Throughput Bubble Screening Method for Combinatorial Discovery of Electrocatalysts for Water Splitting." *ACS Combinatorial Science* 16 (2):47-52.
- Yamashita, Hiroya, Yamamura, Takeshi and Yoshimoto, Katsutoshi. (1993). "The Relation Between Catalytic Ability for Hydrogen Evolution Reaction and Characteristics of Nickel-Tin Alloys." *J. Electrochem. Soc.* 140:2238-2243.
- Zhan, Zhaoyao, Jianing An, Yuefan Wei, Van Thai Tran, and Hejun Du. (2017). "Inkjet-printed optoelectronics." *Nanoscale* 9 (3):965-993. doi: 10.1039/C6NR08220C.